APPLICATION OF INTEGRATED GEOPHYSICAL METHODS FOR GRAPHITE EXPLORATION IN GARA-GEDEMSA AREA (MOYALE, SOUTHERN ETHIOPIA)

A thesis presented to the School of Graduate Studies of
the Addis Ababa University
in partial fulfillment of the requirement for the degree Master of Science
in Geophysics

By

Alemna Jaleta

Addis Ababa
1997

DEDICATION

This work is thoroughly dedicated to my father whom I lost on 30th of July 96, while working towards my master degree.

ACKNOWLEDMENT

The writer expresses his deep gratitude to Dr. Tigistu Haile, the advisor, and Dr. Getnet Mewa, the co-advisor, of this thesis work for their valuable advice and guidance, and for commenting on the thesis. The writer is also greatly indebted to Dr. Tilahun Mammo for his unreserved assistance. Very special thanks are due to W/o Danbele Kanaa for her financial and valuable moral support, and for her mother care. Special thanks also go to Prof. Roberto Balia, Dr. Fekadu Kebede and Dr. Abera Alemu, for their valuable encouragement. Many thanks are due to Ato Belayneh Mesfin and Ato Solomon Beneberu for their friendly encouragement and sharing burdens.

The writer is very thankful to the Ethiopian Institute of Geological Surveys for releasing the raw data used in this work, for providing transportation to access the study area to collect additional data and for providing the printing facilities. The financial assistance received from the Ethiopian Adventist College and the Association of Geoscientists for International Development (AGID) are also acknowledged.

Above all, let the acknowledgment and the glory be unto God for His unceasing care and strengthening all the way through.

TABLE OF CONTENTS

LIST OF TABLES

LIST OF FIGURES

ABSTRACT

The thesis research was aimed at studying the theoretical and practical aspects of the Radiometric, Magnetic, Electromagnetic, Induced Polarization (IP) and Resistivity methods and apply the integrated methods for graphite exploration in the Gara Gedemsa area. The physical principles and mathematical foundations, fields of applications and principles of data acquisition and interpretation of each method are studied in detail.

Integrated geophysical survey, comprising the Radiometric, Magnetic, GENIE-EM, IP and Resistivity methods, was conducted in the Gara Gedemsa area to map the lateral and vertical distributions of the graphitic mineralization. The area is located in Southern Ethiopia some 6 km northwest of Moyale town. Geologically, this area is mostly covered by mafic-ultramafic rocks (talc-tremolite, talc-tremolite-actinolite and amphibole schists), whereas quartzite, quartz-mica schist and pegmatite veins that are closely distributed with the graphite schists are found to have relatively smaller distribution.

The geophysical survey results have delineated one major graphitic zone at the southern margin of the survey grid with strike length more than 2 km along $W30^0N$ and an average width varying from 25 m to 50 m. From the pole-dipole IP/Resistivity and GENIE amplitude ratio data, this graphitic body is found to be dipping towards north at about 55^0 and extends to a depth of not less than 50 m. This graphitic zone is almost equally demarcated by all methods employed for the survey. However, the GENIE-EM survey with the 50 m transmitter-receiver spacing has shown better resolution in discriminating the parallel graphitic lenses closely separated by the nonconductive quartz-mica schists.

A less prominent graphitic zone is outlined at the central part of the grid, and from exploration point of view, it deserves less interest due to its smaller lateral distribution and low anomaly-to-background contrast. Based on the geophysical survey results, a generalized physico-geological model of the Gara Gedemsa graphite occurrence is generated. Moreover, two bore holes are recommended over the main graphitic zone in order to confirm its depth extension and thereby evaluate the economic significance of the deposit.

1. INTRODUCTION

1.1 General

1.1.1 Geophysical Methods for Mineral Exploration

The ultimate target of any exploration activity, whatever the method applied, is to discover mineral deposits serving as raw materials for industries and for other purposes. This principal target may be achieved by application of integrated geological, geophysical and geochemical methods of prospecting which are to be followed by mining and drilling operations. However, the discovery of mineral deposits that are concealed at a larger depth is found to be a difficult task for geological and geochemical methods of exploration. In such conditions, the geophysical methods, which are based on the study of the distribution of physical fields naturally existing or artificially created within the ground hosting the buried deposits, provide better opportunities.

In modern exploration work, different geophysical methods like magnetics, radiometry, electrical and electromagnetics, gravity, seismic and others are applied to search for mineral deposits.

The choice of an area for a geophysical investigation is often dictated by geological considerations. On the other hand, the decision as to which of the geophysical methods are to be used in an area primarily depends on the expected contrast in the physical properties (magnetic susceptibility, electrical resistivity, electrical polarizability, radioactivity, density, etc.) of the ore bodies and the rocks in which they are found embedded. The physical property contrast between an ore body and the host rock is mainly determined by the mineralogical compositions, size and depth of the ore body [6,22].

A geophysical search for an ore body may be conducted in two different ways: the direct and indirect search. A direct search is possible when the measured physical fields are direct

1.1.2. Prospecting for Graphite Deposits

Graphite is a mineral variety of the chemical element carbon. It is one of the softest minerals, and is formed chiefly out of organic carbon in rocks under high temperature conditions. Its ore are usually subdivided into two groups: a) cryptocrystalline or amorphous graphite- which is formed from coal seams that have undergone contact metamorphism; and b) phanerocrystalline graphite- derived from organic matter disseminated in heavily altered sedimentary rocks which have been converted by high temperatures and pressures into gneisses and crystalline schists. Deposits of phanerocrystalline graphite are associated with metamorphic and igneous rocks (gneisses, crystalline schists, marbles, granites, etc.), while cryptocrystalline deposits occur between series of sedimentary rocks (sandstones, clayey schists, limestones) [8,9].

Commercially, graphite serves as a raw material in the manufacturing of crucibles and other refractory products, for making lubricant, brushes for electric motors, foundry facings, pigments, batteries and pencils. It is also used in atomic reactors to slow down the neutrons [9]. These and other uses of graphite necessitate the exploration for it.

Graphite is mainly characterized by its softness. Besides, it soils fingers, marks paper and is greasy when touched. These properties are used to identify it in the field [9]. Considering its physical properties, graphite has low susceptibility, high conductivity and also high chargeability; and often these features make it anomalous relative to its host rocks [21,20]. Thus, the magnetic, the electrical and the electromagnetic methods can be suitably applied to delineate graphitic bodies.

1.2 Geophysical Explorations in the Survey Area

1.2.1 Location and Accessibility of the Survey Area

The Moyale graphite occurrence is situated about 5-6 Km north-west of the Moyale town near Ethio-Kenyan border within the Oromiya region (Fig. 1).

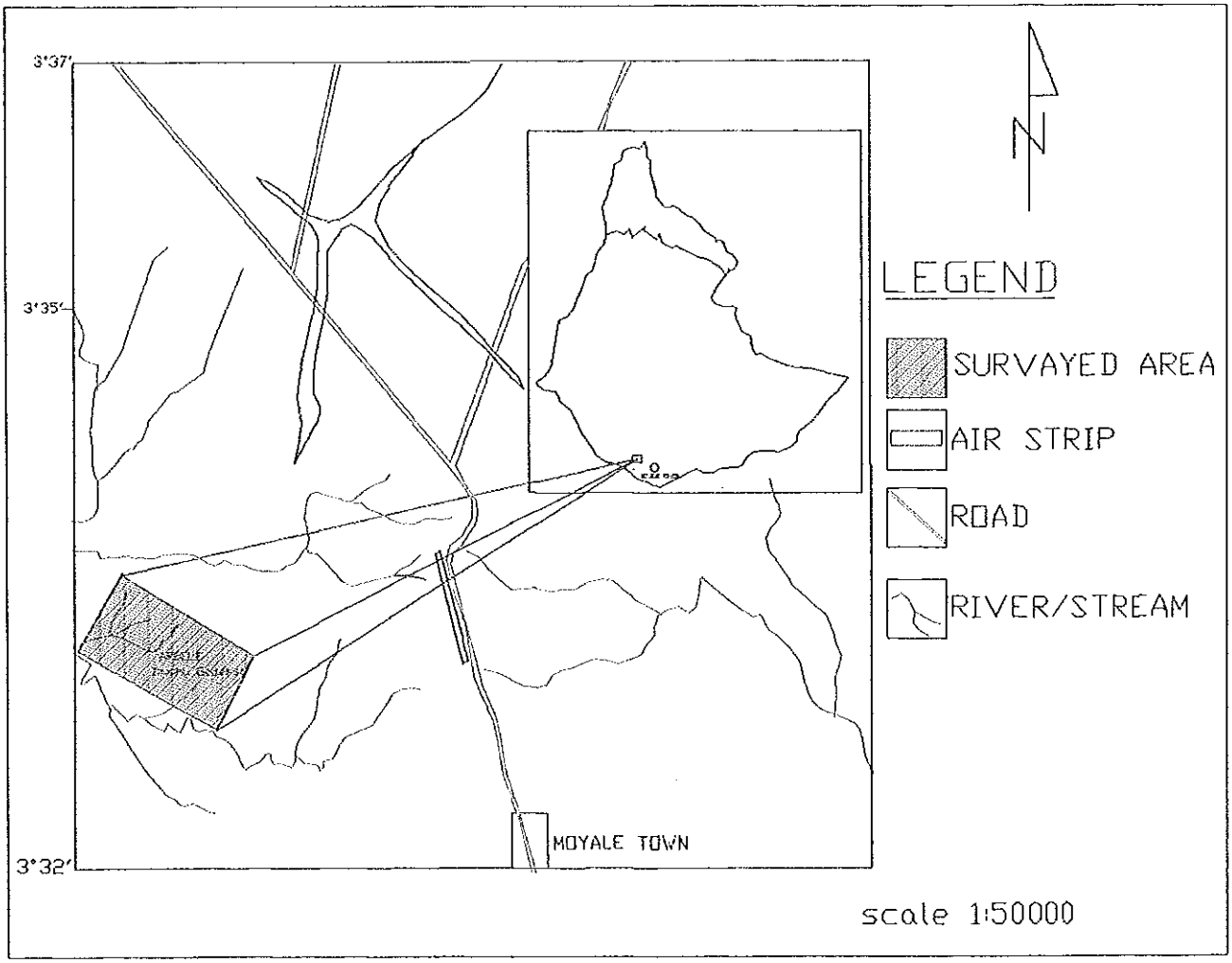

Fig. 1. Location map of Gara Gedemssa Area.

Geographically, the area is located between 3°32'23"N/38°59'55"E and 3°33'43"N/39°01'46"E with elevation ranging from 1100 m to 1300 m above mean sea level and covering a total area of 2.4 sq. km. The topography is rugged and is vegetated with small bushes and trees. The climate is very hot during summer and moderate in the winter.

The area is accessible via a 770 km Addis Ababa-Moyale asphalt road and a detour of 5-6 km dry weather road.

1.2.2 Objectives

The aim of the present research is to study the theoretical foundations and practical applications of the geophysical methods that are often used in mineral exploration, and apply integrated techniques for exploration of graphite deposit in the Gara-Gedemsa area.

The objectives of this thesis research were, therefore:

- to study the theoretical foundations and practical applications of integrated geophysical methods consisting of magnetics, radiometry, electrical & electromagnetics for mineral. in particular for graphite, exploration in the Gara-Gedemsa area;
- to carry out petrophysical analysis, such as magnetic susceptibility, chargeability and apparent resistivity of the main rock units of the study area and work out criteria for field data interpretation;
- to map the lateral distribution, depth extension and strike and dipping direction of the graphite mineralization within the survey area;
- to detect and identify geological structures, such as faults, fractures (shear zones), folds, litho-contacts, etc. as possible sites of graphite and other associated mineralization; and
- to compile a generalized physico-geological model, representing the mineralized zone of the study area, that may be applied in other areas with similar geological setting.

1.2.3 Methods of Approach

To achieve the objectives set above, geophysical studies were carried out in the survey area along twenty one profiles laid perpendicular to the assumed strike of the target body. During the course of the field survey, chargeability (M), apparent resistivity (ρ_a), total magnetic field (T), amplitude ratio of vertical magnetic field and intensities of natural gamma radiations (Total Count, K, U, Th) were measured and/or indirectly determined. For reliable interpretation and correlation of the geophysical results, the different physical parameters were measured along the same profiles. In addition, analysis of the rock's magnetic susceptibility, apparent resistivity and chargeability were performed using rock samples collected from the field and measured data so as to work out criteria for further geophysical data interpretation. The interpretations are made from the generated contour and pseudosection maps, and profile curves of the field data. Finally, the results are integrated with the available geological information on whose basis conclusions are forwarded regarding the abundance and economic significance of the graphite deposit.

Accordingly, the next four chapters present a theoretical description, methodologies of the field works and field results, including data analysis, presentation and interpretation of each of the method used in the survey. In presenting the results, the coordinates of the maps and profile curves are named assuming the profiles to lie along north-south direction, only for simplicity. Geographically, the profiles lie along N30^{0}E, whereas the base line lies along W30^{0}N. The strike direction of the target body is defined with respect to geographic north. In the last and concluding chapter, the integrated interpretation of the field data is carried out. The geology and petrophysical analysis of rocks from the study area are presented in the following section.

1.3 General Geology of the Survey Area

1.3.1 Geology and Mineralization

The geology of Moyale area has been studied at different times by different investigators. However, more recently a regional geological map at a scale 1:50 000 was compiled by Tolosa S. et al. [22]. Accordingly, the Gara-Gedemsa and its surrounding areas are bounded by a granodiorite complex which at places is intersected by NNE-SSW running faults. Graphitic schists and mafic-ultramafic rocks are sandwiched by this granodiorite complex.

Detailed geological mapping has commenced in 1995 in conjunction with the geophysical surveys employing the Magnetics, Radiometry, Resistivity and Induced Polarization methods. As shown on the 1:10 000 scale geological map in Fig. 2, the majority of the Gara-Gedemsa area is covered by mafic-ultramafic rocks that are represented by talc-tremolite, talc-tremolite-actinolite as well as amphibolite schists. In addition, pegmatite veins are commonly encountered at the northwest-central and southern margins of the grid. At different localities, quartzites and quartz-mica schists intercalated with graphitic zones are mapped. At the north-west of the grid occurrences of quartz veins are also mapped.

As far as the mineral occurrences are concerned, so far graphite seems to be the most abundant mineral expected to deserve exploration interest. Geologically, two zones are reported to be associated with graphite mineralization - one at the southern margin, and the other at the central part of the grid. At some places within these zones, graphite is observed exposed on the surface.

A brief petrographic study of graphite from the Moyale area by Gautneb H. [6] has indicated that the graphite is well crystallized and flaky and is oriented parallel to the foliation in the graphite schist. The graphite ore is assumed to be derived from organic matter disseminated in heavily altered sedimentary rocks, which have been converted by high temperatures and pressures into crystalline schists. The pegmatite veins mapped in association with the graphite schists could be the result of late cooling of the molten igneous masses that rose from the depths of the earth, which might have caused the graphitic alteration.

Within the present area of survey, next to graphite, talc may be considered as the second target of industrial mineral exploration.

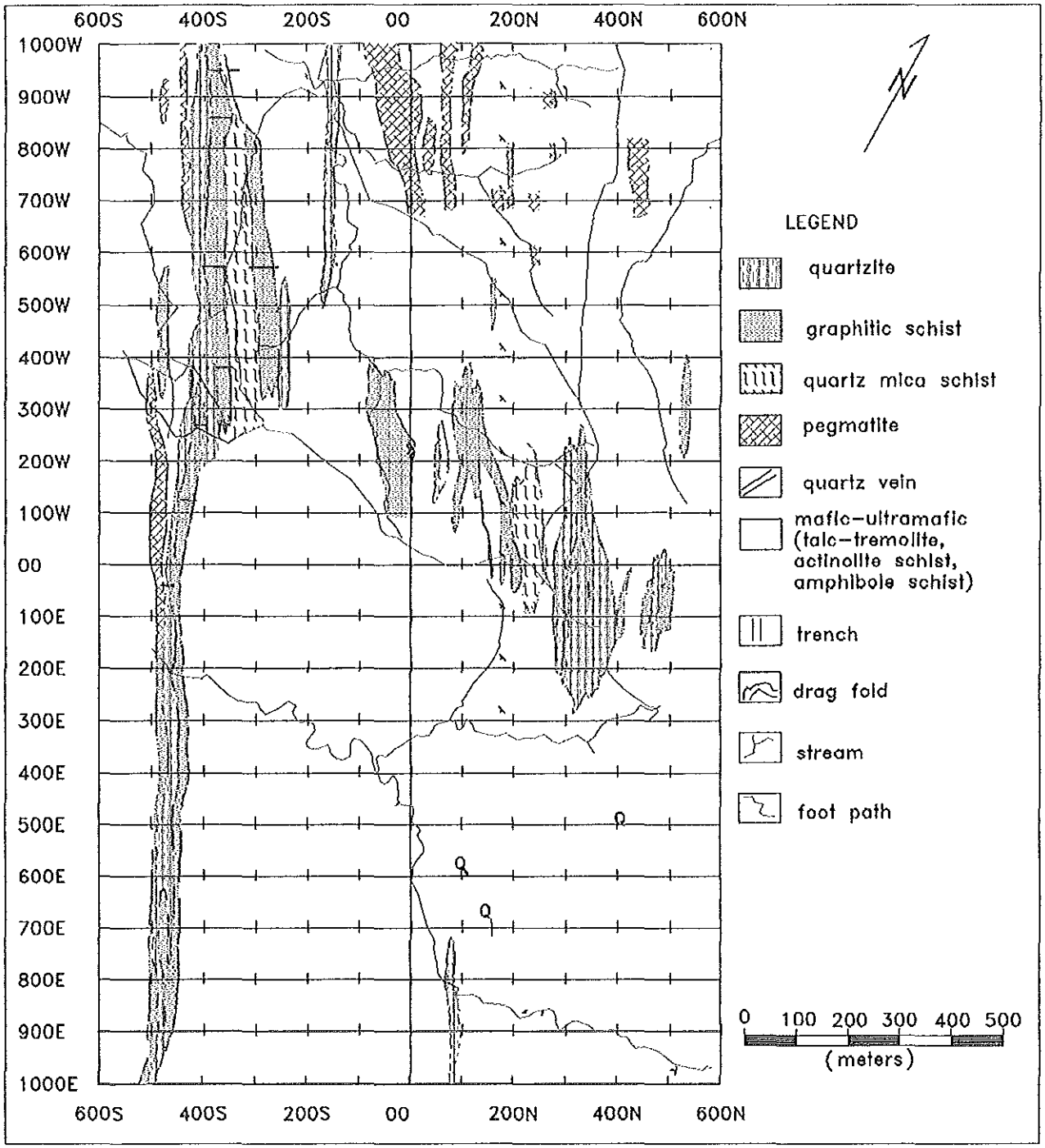

Figure 2. Geology and survey grid of Gara Gedemsa.

1.3.3 Petrophysical Analysis of Rocks from the Study Area

The susceptibility measurements made using a core testing unit (CTU-2) for rock samples collected from the field, mainly along the expected anomalous zone, have indicated susceptibility readings in the order of 10^{-8} to 10^{-5} cgs. The graphite samples displayed low susceptibility values relative to the host rocks (quartzite, pegmatite, and mafic-ultramafic units represented by talc-tremolite and talc-tremolite-actinolite schists). On the other hand, the chargeability and resistivity of the major rock units of the area were estimated from the physical parameters measured in the field using the central gradient array with the current and the potential electrodes spacings of 1480 and 20 meters respectively. Accordingly, the graphite schist is represented by high chargeability and low resistivity relative to the host rocks. These physical property contrasts allow to delineate the graphitic zone geophysically. The results are presented in Table 1.

Table 1. Physical properties of major rock units of the survey area

Type	Susceptibility x 10^{-6} cgs	Chargeability (msec)	Resistivity (Ohm-m)
Graphite schist	0.04-0.64	60-180	0-10
Quartzite	0.354-144	20-30	>1000
Quartz-mica schist	0.04-0.354	40-50	5-20
Pegmatite	*	30-40	200-700
Mafic-ultramafic(talc-tremolite, talc-tremolite-actinolite)	0.64-24	0-20	10-1000

The values even vary considerably for the same rock type which could be attributed to some factors like thermodynamic conditions responsible for the alterations, the degree of weathering and the

efficiency of the method used to estimate the values. Physical properties of some rocks and minerals are given in Table 2 for comparison (adapted from [10,18,21]).

Table 2. Physical properties of some rocks and minerals

No	Rock/Mineral type	Susceptibility (x 10^6 emu)		Resistivity (Ohm-m)
		Range	Average	
1.	Amphibolite		60	
2.	Graphite schist			10^1 - 10^2
3.	Quartzite		350	10 - 2 x 10^8
4.	Gneiss	10-2000		2.5 x 10
5.	mafic (talc schist, amphibolite schist)	100-1000		5-100
6.	Pegmatite	3000-75000	5000	
7.	Granite	0-4000	400	5.0 x 10^3 -3.6 x 10^6
8.	Granodiorite			6.8 x 10^4
9.	Graphite		-8	10^{-7} -10^1
10.	Quartz		-1	4 x 10^{10} -2 x 10^{14}
11.	Magnetite	10^5-1.6x10^6	5 x 10^5	5 x 10^{-5} - 5.7 x 10^3

2 RADIOMETRIC METHOD

2.1 Basic Theory

Radioactivity: The nuclei of certain elements disintegrate spontaneously emitting energetic corpuscular and electromagnetic radiation and, in doing so, are transformed into nuclei of other elements. The alpha (Helium nuclei) and beta (positron or electron) particles and gamma (γ) radiation are emitted from the process. This phenomenon of spontaneous disintegration and emission of radiation is known as radioactivity. Of the three radiations, the gamma (γ) radiation is successfully used for exploration purposes due to its better penetration power. Although about fifty naturally occurring elements are known to be radioactive, only uranium (U), thorium (Th) and an isotope of potassium (K) are found to be important for exploration purposes [21].

The disintegration of a given quantity of any radioactive element is expressed by the exponential law

$$N = N_o e^{-\lambda t} \qquad (1)$$

where No - is the number of nuclei initially present, N the number of nuclei remaining after time t and λ is the decay constant.

The half-life ($T_{1/2}$), the time during which half the atoms of a nuclei disintegrate, is given by

$$T_{1/2} = \frac{0.693}{\lambda} \qquad (2)$$

Radioactivity of rocks: The radioactivity of rocks is dependent upon the amount of uranium and thorium and their daughter products like radium, polonium, radon, etc. present in them. Uranium occurs in acidic and alkaline rocks, like granites and pegmatites, in the form of a mineral called uraninite. Certain metaliferous veins enriched with minerals like tin, copper, lead and silver may contain uranium, sometimes in appreciable quantities. In addition, uranium may occur in

2.4 Data Processing, Presentation and Interpretation

Data Processing and Presentation: Owing to the γ-rays in cosmic radiation and the atmosphere, and also the general radioactivity of rocks, there is always a background count which must be determined in every survey area so as to evaluate the anomaly/background ratio and perform data interpretation.

The result of the radiometric survey is displayed as contour maps in counts/3 seconds. The field data for each channel (Total Count, K, U, Th) was first gridded at 5-units cell size and then contoured using the "geosoft" mapping and processing system. The Total Count contour map is prepared using contour intervals of 25 and 50 counts/3 sec and compiled at the scale of 1:10 000, whereas the potassium contour map is generated at the same scale using a 4 counts/3 sec contour interval. Because of the poor anomaly/background contrast of the U and Th measurements, no prominent geological information were recognized from their results. Therefore, presenting the U and Th maps was found unnecessary.

Data Interpretation: On the radiometry total count contour map (Fig. 3) three distinct anomalous zones with enhanced response are observed. Of these zones, the first and the most significant one, with values greater than 70 counts per second (210 counts/3 sec), is mapped at the southern margin of the grid almost along 400 S. As seen from the map, this zone has a strike length of more than 2 km along W30^{0}N with an average width of about 250 meters between profiles 200W and 1000W and thins to about 100 meters in the eastern portion of the grid. The position of this strong radiometric anomaly zone coincides with the distribution of pegmatite veins which have

space relationship with graphite mineralization. This elongated anomalous zone is open to the west and east indicating the continuation of a similar formation beyond the surveyed grid.

The second anomalous zone, detected at the central part of the grid between 200W/0 and 200E/500S with east-west strike direction (Fig. 3), is characterized by moderate to high values (50-100 counts/sec). Geologically, small pegmatite veins intercalated between graphitic schists are assumed to be responsible for the circular patches of anomalies encountered within this zone.

The third anomalous zone with moderate response (50-85 counts/sec) is detected between 500W/200S and 1000W/200S. The position of this moderate radiometry zone and the oval shape anomaly with a relatively higher response (70-100 counts/sec) observed within this zone at 1000W/100S also coincides with the distribution of pegmatite veins which could cause the anomaly. The areas of low radiometric response (less than 50 counts/sec) observed on the map represent mafic-ultramafic units such as talc-tremolite, talc-tremolite-actinolite and amphibolite schists.

Similar to the total count, the potassium measurements (Fig. 4) have roughly outlined the main lithologic units of the survey area, more or less, following the same trend. The anomalous zone along the southern margin of the grid, detected by the total count measurements, is characterized by potassium radiation intensities in the range of 3-8 counts/sec. The central and northwest anomalous zones are represented by moderate values in the range of 2.5-5 counts/sec. The mafic-ultramafic units represented by talc-tremolite, talc-tremolite-actinolite and amphibolite schists, have relatively shown low potassium radiation intensities, less than 2.5 counts/sec, with some distribution of moderate values.

Generally, from the radiometric survey data, it may be concluded that the sources of the observed anomalies are bodies with high content of potassium such as pegmatites and/or zones that have undergone potassium alteration which may have genetic relation with graphitic schists.

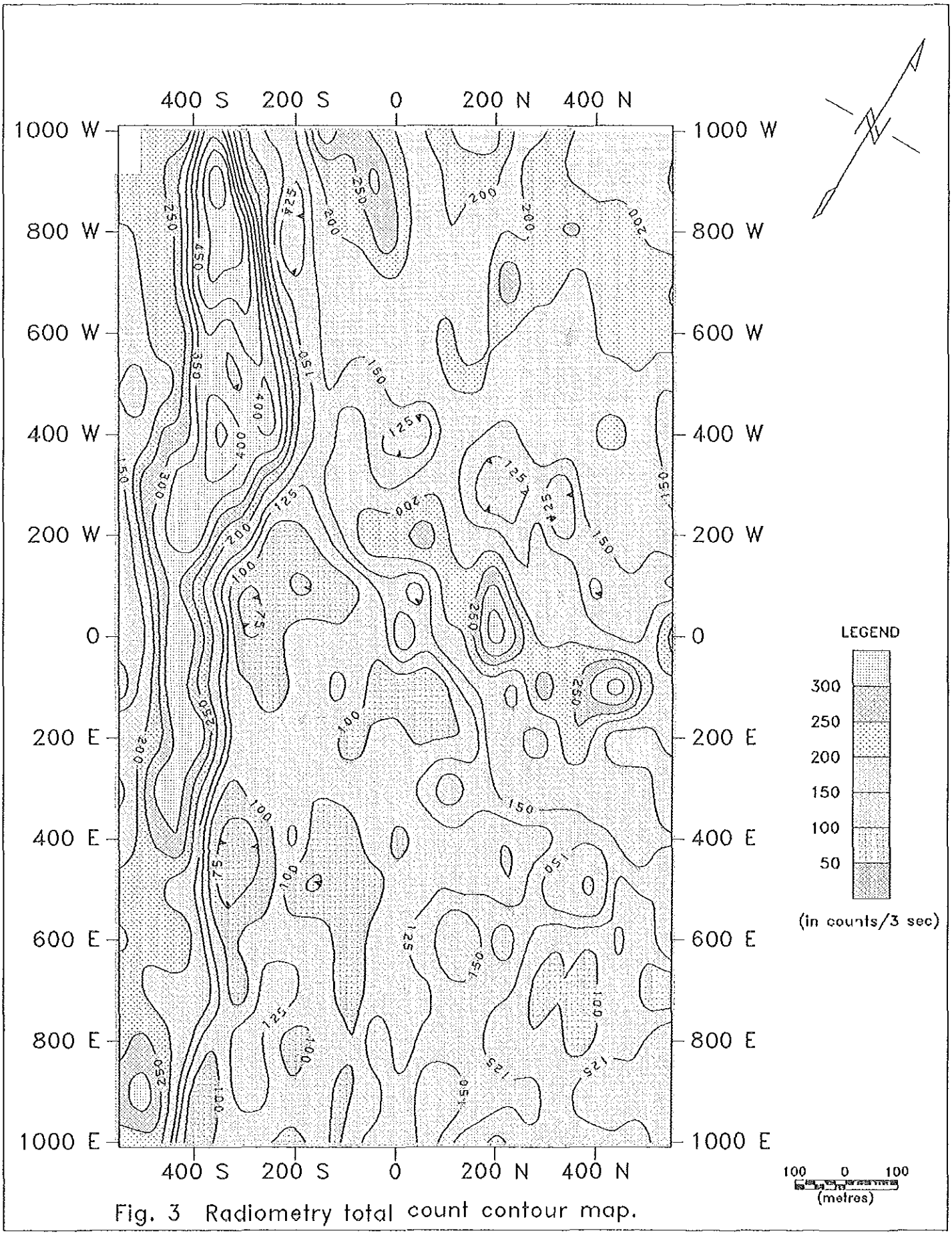

Fig. 3 Radiometry total count contour map.

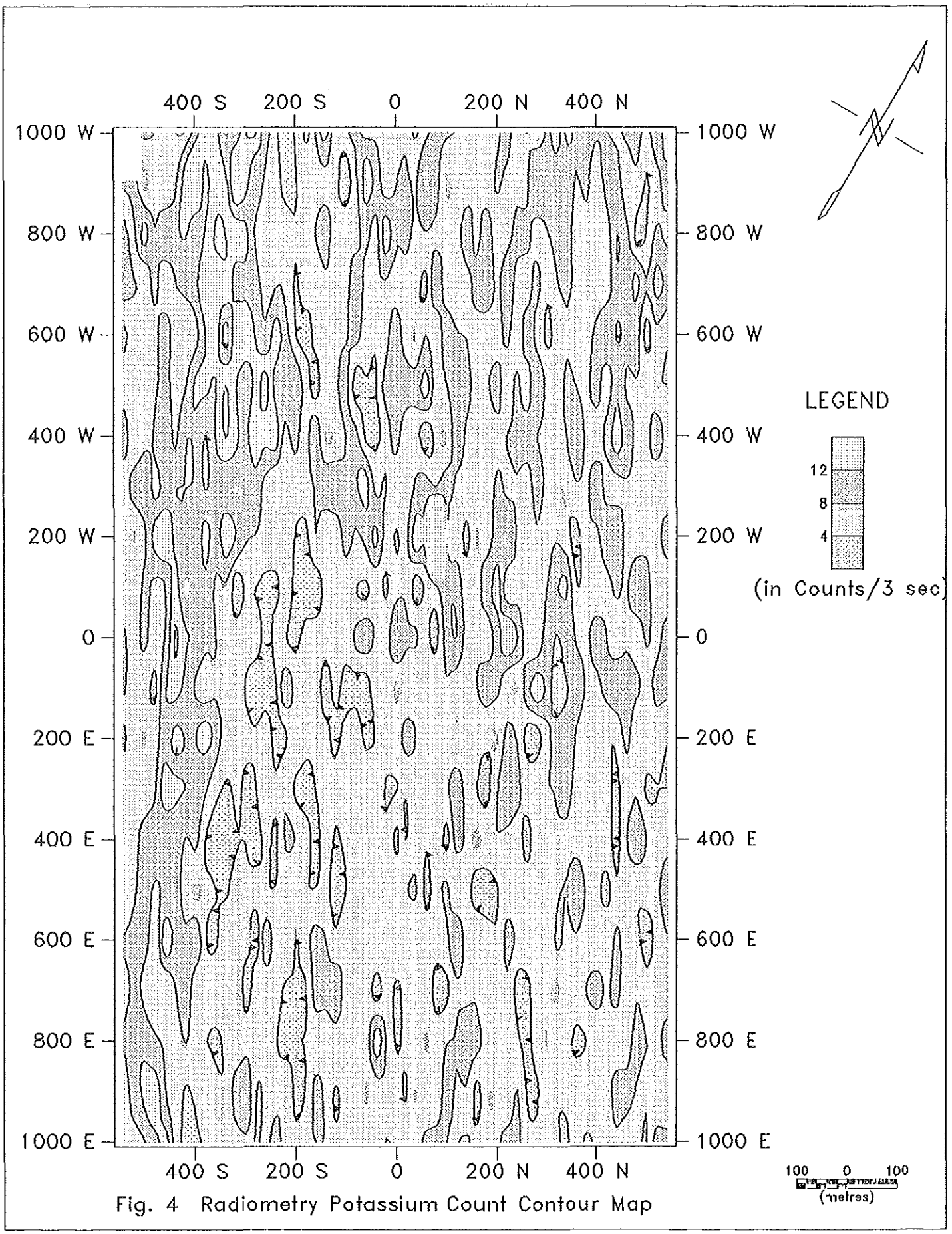

Fig. 4 Radiometry Potassium Count Contour Map

3 MAGNETIC METHOD

The magnetic method of prospecting is the oldest geophysical method and is applied in various degrees for mineral, oil, gas, coal and groundwater explorations as well as for geotechnical and archaeological site investigations [5]. The method is especially effective to map structural features like faults, fractures and/or contact zones which often serve as potential hosts for a variety of minerals and/or conduits for movement of groundwater. In oil, gas and coal exploration the method is mainly used as a reconnaissance tool to assist in outlining and determining the thickness of the sedimentary basin and areal extent of the potential area.

In mining geophysics, the method is applied to locate zones of occurrence of ferrous and non-ferrous mineral deposits such as iron ores, base-metals, sulphides, gold, graphite, asbestos, etc. by measuring the magnetic field variation produced due to the remnant and/or induced magnetization contrasts between the mineralized bodies and the host rock.

3.1 Basic Magnetic Theory

The Earth's Magnetic Field: The knowledge of the earth's magnetic properties and conditions of the earth as a whole is necessary as magnetic measurements are made within the magnetic field of the earth. The earth's magnetic field at a given place and time is believed to have:

- an external origin - which is due to the solar wind, a constant stream of ionized particles emitted from the sun. It makes 0.5% of the field and is the cause for the diurnal variation of the total field;
- an internal origin - which is due to magnetic field of the dipole field generated at the outer core;
- magnetism of rock's- associated with geological structures. Magnetic field variations produced due to this field is the chief interest in magnetic prospecting and it designates the anomaly part.

The earth's total field intensity is not perfectly symmetric about the geographical poles due to local variations in the distribution of magnetic minerals within the earth's crust. The field variation with time is also observed due to the effect of solar wind that reaches in the range of 50-100 nT and magnetic storms in the order of 50 nT as they distort the magnetosphere or the external magnetic field of the earth. The earth's internal or main field also changes slowly over many years through what is termed as the secular variation. The inclination, intensity and even the location of the poles varies slowly [2,14]. To isolate the anomaly part, that is, the field due to local magnetized bodies within the earth's crust, the main field and the diurnal parts must be removed as the geomagnetic observation is necessarily affected by the sum of all the three parts.

Magnetic field strength: The force $\vec{F}$ between two poles with strength P_0 and P separated by a distance r is expressed as

$$\vec{F} = \frac{\mu_0}{4\pi\mu_r}\frac{P_0 P}{r^2} \tag{3}$$

When $\vec{F}$ is in Newtons, P in ampere-meters and r in meters, μ_0, the permeability of free space, is given in Newton per square ampere ($N.A^{-2}$). μ_r is the relative permeability of the medium separating the poles, and is dimension less. The magnetic field strength at a point is defined as the force per unit of pole strength which would be exerted on a small pole of strength P_0 if placed at that point. Thus, the field strength $\vec{H}$ due to a pole of strength P at a distance r is given as

$$\vec{H} = \frac{\vec{F}}{P_0} \text{ or } = \frac{\mu_0 P}{4\pi\mu_r r^2} \tag{4}$$

where $\vec{H}$ is in Ampere per meter.

Magnetic Induction: A magnetic body when placed in an external field $\vec{H}$ has its internal poles more or less lined up by the field $\vec{H}$ to produce a field of its own $\vec{H}'$, which increases the total field within the body. This extra field is related to the intensity of magnetization I as [17].

$$\vec{H}' = 4\pi \vec{I} \qquad (5)$$

where the induced intensity of magnetization $\vec{I}$, i.e., the magnetic moment per unit volume, acquired by the body due to a magnetizing force $\vec{H}$ is given by

$$\vec{I} = K\vec{H} \qquad (6)$$

where K is volume susceptibility of the body.

The intensity of magnetization is an important property of rocks which has great significance in magnetic prospecting.

The magnetic effect of a homogeneously magnetized body depends on the grain size of the magnetic minerals, their distribution within the rock mass and also the direction of magnetization.

The magnetic induction $\vec{B}$ is defined as the total field with in the body, i.e.,

$$\vec{B} = \vec{H} + \vec{H}' \qquad (7)$$

Substituting for $\vec{H}'$ from eqns. (5) and (6),

$$\vec{B} = (1 + 4\pi K)\vec{H} \qquad (8)$$

where $(1 + 4\pi K) = \mu$ is the relative magnetic permeability. $\vec{H}$ an intrinsic magnetic strength and $\vec{B}$ represents the induced magnetic field plus an intrinsic magnetic field.

In SI system of units $\vec{H}$ is measured in Ampere per meter, whereas $\vec{B}$ is in Weber per square meter. In the cgs system, where one unit of electric current (absolute-ampere) is 10 ordinary Ampere, i.e., 1 ab Ampere = 10 Ampere, magnetic induction $\vec{B}$ is measured in Gauss (G) and $\vec{H}$ - in Oersted. Because these units are large, a nanotesla (nT) or gammas (γ) is used to measure the magnetic field strength in magnetic prospecting [17,21].

$1\gamma = 10^{-5}$ G = 1 nT

Earth's Magnetic Field Elements: The direction and magnitude of the geomagnetic field at any point on the earth's surface are represented by a vector parallel to the direction of the field pointing in the direction of force on a positive pole and having a length proportional to the strength of the field at that point. This vector is referred to a set of mutually perpendicular axes directed astronomically north and east and vertically downward (Fig. 5).

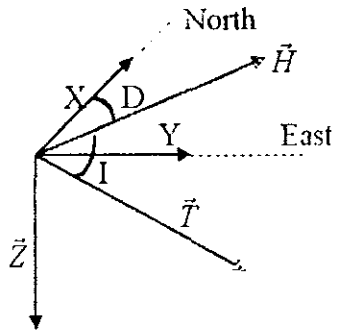

Fig. 5 Earth's magnetic field elements

The total field (T), the vertical (Z) and the horizontal (H) components of the total field, the inclination (I) and declination (D) are important components involved in magnetic prospecting [2]. The magnetic elements as illustrated in Fig. 5 are related as follows:

$$H = T\cos I \qquad X = H\cos D \qquad X^2 + Y^2 = H^2$$

$$Z = T\sin I = H\tan I; \qquad Y = H\sin D \qquad H^2 + Z^2 = T^2 \qquad (9)$$

where X and Y are the horizontal components of vector $\vec{H}$.

These quantities can also be derived from magnetic potential V. In spherical coordinates, the vertical (Z) and horizontal (H) components of the total field (T) are defined as

$$Z = \frac{\partial V}{\partial r}; \quad H = \frac{1}{r}\frac{\partial V}{\partial \theta} \qquad (10)$$

where $\vec{T} = \vec{Z} + \vec{H}$

For example. assuming a dipole of potential $V = (\mu_0/4\pi)\, M \cos\theta / r^2$ located at the center of the earth, the horizontal and vertical components of the total magnetic field at an external point of distance r from the center is derived from the potential as follows (Fig. 6):

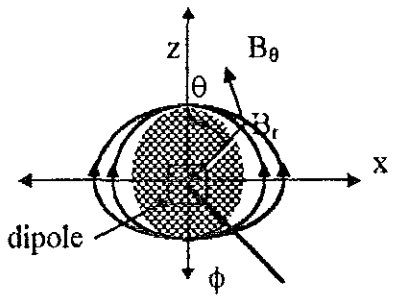

Fig. 6. Schematic representation of the earth's magnetic field

$$B_\theta = H = \frac{1}{r}\frac{\partial V}{\partial \theta} = \frac{\mu_0 M \sin\theta}{4\pi r^3} \qquad (11)$$

$$B_r = Z = \frac{\partial V}{\partial r} = \frac{2\mu_0 M \cos\theta}{4\pi r^3} \qquad (12)$$

where M =2lp (l the dipole length) is the magnetic moment, and θ the magnetic latitude.

Substituting for μ_0 (= $4\pi \times 10^{-7}$ N/A^2), M (= 7.9×10^{22} Am^2), and r (= 6.4×10^6 m, for the radius of the earth) in eqns. (11) and (12), the horizontal and vertical components of total magnetic field are nearly 0 and 60,000 nT, respectively, along the north pole (θ = 0^0) and the south pole (θ = 180°). Thus, at polar regions the total field has only vertical component. On the other hand, at the equator where θ = 90°, the magnitudes are 30,000 nT and 0 for the horizontal and vertical components, respectively. Here the total field has a horizontal component which is only half the magnitude at polar regions.

Magnetic Properties of Rocks: The magnetism of practically all rocks is controlled by their content of magnetic minerals like magnetite, hematite, pyrrhotite, ilmenite and some others. Magnetite is by far the most magnetic and the most common. Although the variation of

susceptibilities is considerable, it is possible to generalize that magnetite, pyrrhotite, ilmenite and some chromite and manganese-bearing ores have large susceptibilities; while pyrite, zinc, and galena are characterized by lower susceptibility values. Minerals such as graphite and quartz have negative susceptibility values. Rocks like basalts, diabases, skarns and some granulites as well as pegmatites are much more magnetic than sedimentary rocks like limestones, sandstones and slates [2,14]. Magnetic susceptibilities of some rocks and minerals are given in Table 2.

3.2 Magnetic Anomaly

A magnetic anomaly represents a local disturbance in the earth's magnetic field which arises from a local change in magnetization or a magnetization contrast. The form of the magnetic anomaly from a given body depends on factors such as: the geometry of the body, the direction of the earth's field at the location of the body, the direction of polarization of the rocks forming the body, the orientation of the body with respect to the direction of the earth's magnetic field, the orientation of the line of observation with respect to the axis of the body, etc. [14]. Magnetic anomalies in the earth's field are caused by two different kinds of magnetism - the induced ($\vec{I}_i$) and the remnant ($\vec{I}_r$) magnetizations. Thus, total magnetization ($\vec{I}$) is a vector sum of the induced and remnant magnetizations, i.e.,

$$\vec{I} = \vec{I}_i + \vec{I}_r \qquad (13)$$

$\vec{I}_i$ depends on the susceptibility of the body, whereas $\vec{I}_r$ on the geologic history of the rocks.

Practically, the sources of magnetic anomalies (ΔT) are the existence of ferromagnetic minerals in the crust of the earth. The contrasting proportion of these ferromagnetic minerals makes the anomaly defined as

$$\Delta T = T_{obs} - T_o - T_{sw} \qquad (14)$$

where T_{obs} - is the total magnetic field as measured by the survey magnetometer, T_o the magnetic field due to dipole, determined from the IGRF (the International Geomagnetic Reference Field) and T_{sw} is the magnetic field due to solar wind determined from magnetogram or a base station magnetometer.

The magnitude of the magnetic anomaly ΔT (the component of the anomalous field in the direction of undisturbed total field), can also be expressed interms of its components (see Appendix A for the derivation), i.e.,

$$\Delta T = \Delta H \text{ Cos I Cos } \alpha + \Delta Z \text{ Sin I} \qquad (15)$$

where ΔH and ΔZ are the horizontal and vertical components of the change in total field due to the local disturbance; I the inclination, and α the profile azimuth or angle between the profile and horizontal. This relation is used in modeling magnetic data for determining the parameters of the anomalous body such as depth, shape, size and dip [2].

Eqn. (15) can be used to calculate the magnetic anomaly due to simple geologic structures like a dipole and a monopole at any magnetic latitude. For example, for a dipole located at the north pole (where I = 90°) (Fig. 7) it yields the following signature (assuming α to be zero):

$$\Delta T = \Delta Z = \frac{M(2Z^2 - X^2)}{(X^2 + Z^2)^{5/2}} \qquad (16)$$

Similarly, at the equatorial region, where I = 0^0, it yields

$$\Delta T = \Delta H = \frac{M(2X^2 - Z^2)}{(X^2 + Z^2)^{5/2}} \qquad (17)$$

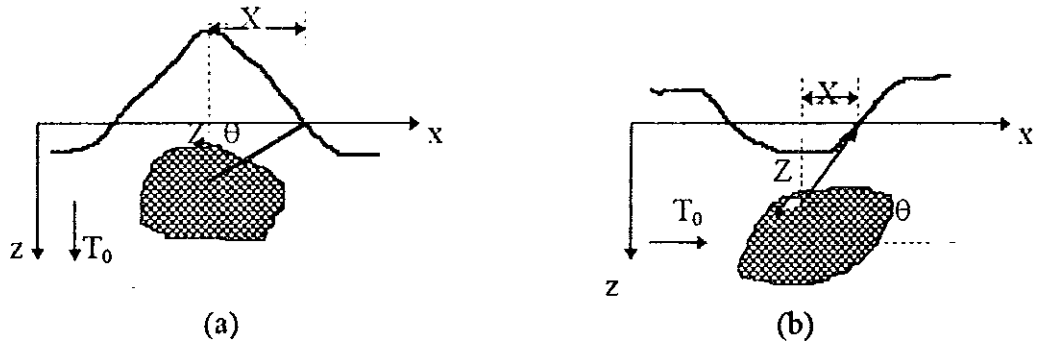

Fig. 7. Magnetic anomaly due to dipole a) at north pole and b) at the equator

The maximum amplitude of the magnetic anomaly over the earth's surface is a function of the depth and contrast in the mass of magnetic minerals and, to a less extent, on the configuration of the source [2]. The basic expression for estimating the maximum amplitude of any anomaly is given by

$$\Delta T = \frac{M}{r^n} \qquad (18)$$

where ΔT is the anomaly magnitude, M the magnetic moment, r the distance (depth) to the source, and 'n' a measure of the rate of decay of the field with distance, or fall-off rate (n=3 for a dipole, n=2 for a monopole, etc.) [2].

The end result of a magnetic survey is an anomaly magnitude plot along a set of profiles or a magnetic contour map. Qualitatively the interpretation can be done by looking at the magnetic maps and delineating anomaly patterns. Successive circular closed contours with anomalies increasing or decreasing show a certain geologic structure with either positive or negative anomaly. The direction of elongation of closed contours indicate the strike direction of the anomalies. High horizontal gradients are associated with contacts between rocks of different susceptibility and these may also indicate shallow anomalous bodies. An anomaly of large areal extent may be due to a large weakly magnetized shallow structure or a strongly magnetized small body at a greater depth.

horizontal components of the total field, as well as the declination and inclination of the magnetic fields. For the present study, a proton-precession magnetometer, IGS-2/MP-4, is used to measure the total magnetic field. The total field measured by the proton-precession magnetometer is the sum of the unperturbed field (T_o) and the component of the local disturbance ($\Delta T_{\parallel}$) parallel to the unperturbed field, i.e., $T_o + \Delta T_{\parallel}$ (Fig. 8).

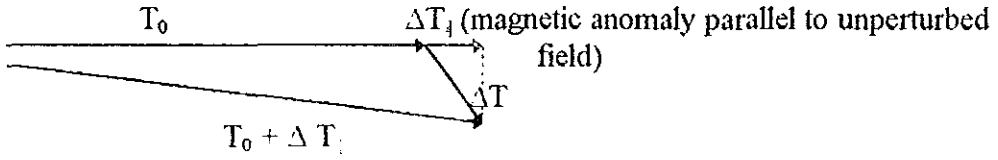

Fig. 8 Local perturbation of the total field vector

The IGS-2/MP-4 has a resolution of 0.1 nT and a 2 seconds reading-time to sense a slight variation in the rocks magnetism [15]. The total field measurements were carried out along the 22 profiles selected for the other surveys and readings were taken at every 20 meter station interval. Every day, before commencing the actual data acquisition and at the end of the daily survey, the base station readings were taken for diurnal correction. The sensor was mounted on a back-harness in such a way that the polarizing field of the coil is pointing vertical and a tuning field of 34000 nT was selected as required by the geographic location of the survey area.

3.4 Data Processing, Presentation and Interpretation

Data Processing and Presentation: Diurnal variations of the earth's magnetic field occur due to solar wind, micropulsations and magnetic storms. The correction for the diurnal variation was made using the readings taken by reoccupying the base-station chosen within the survey area where the field is assumed to be normal undisturbed. This was performed using the relation

$\left[(T_2 - T_1)(t_2 - t_1)\right]/(t_2 - t_1)$, where T_1 and T_2 are the base station readings at time t_1 and t_2, respectively, and t_i is the time at which each reading was taken at the station.

The secular variation is corrected by subtracting the applicable IGRF value, updated to the time of survey, from the observed values of the total magnetic intensity [5]. In practice, for investigating magnetic anomaly of an area, the zero-level that is the reading of the instrument at a point where the field is the normal undisturbed geomagnetic field is used [19]. For this particular study the zero value was taken to be the base station reading. The local fields or the anomalies due to magnetism of magnetized rocks were then computed using eqn. (14) from the observed readings. The residual field map was generated with a contour interval of 10 nT at a scale of 1:10 000 using the "geosoft" mapping and processing system.

Data Interpretation: The result of the magnetic survey has some indication over the anomalous zones which were identified from the radiometry data. As seen on the residual magnetic contour map (Fig. 9), the main anomalous zone delineated by high radiometry (Fig. 3) along the southern margin of the survey grid generally displays weak magnetic response (i.e., ΔT less than 0 nT). This low magnetic response lies between 400S and 200S in the western grid and terminates around 600W-700W. In the eastern part of the grid, the extension of the above discussed anomalous zone lies between 400S and 500S with discontinuations at 200E and 800E. The low magnetic response of this zone could be attributed to graphite owing to its poor susceptibility. The discontinuations of the anomaly observed within this zone, mainly in the eastern part of the grid, could be due to a structural disturbance. The high magnetic response introduced in this zone, particularly to the west of profile 600W, may be attributed to pegmatite and the effect of shallow bed rock. The change in anomaly axis observed near 200E, might have caused by some deformations.

The central anomalous zone detected by radiometry survey, close to 0/200N, has no well defined magnetic anomaly trend. However, some patches of anomalies with ΔT values less than

0 nT are detected. Some graphitic bodies are observed at field along this zone which could be the source of the weak magnetic response. The anomalous zone detected with moderate radiometry response at northwest part of the grid has shown disturbed magnetic response. The high magnetic response of this zone could be attributed to pegmatite veins and shallow bed rock, whereas the low magnetic response could be assumed to be due to bodies of poor susceptibility found in association. Most of the survey area shows moderate magnetic response which may represent the large mass of mafic-ultramafic rock units such as talc-tremolite, talc-tremolite-actinolite and amphibole schists.

Along profile 500E the magnetic response show some structural disturbances which, of course, has no correlation with the other geophysical results and the surface geology. These discontinuities could be due to weak tectonic zones.

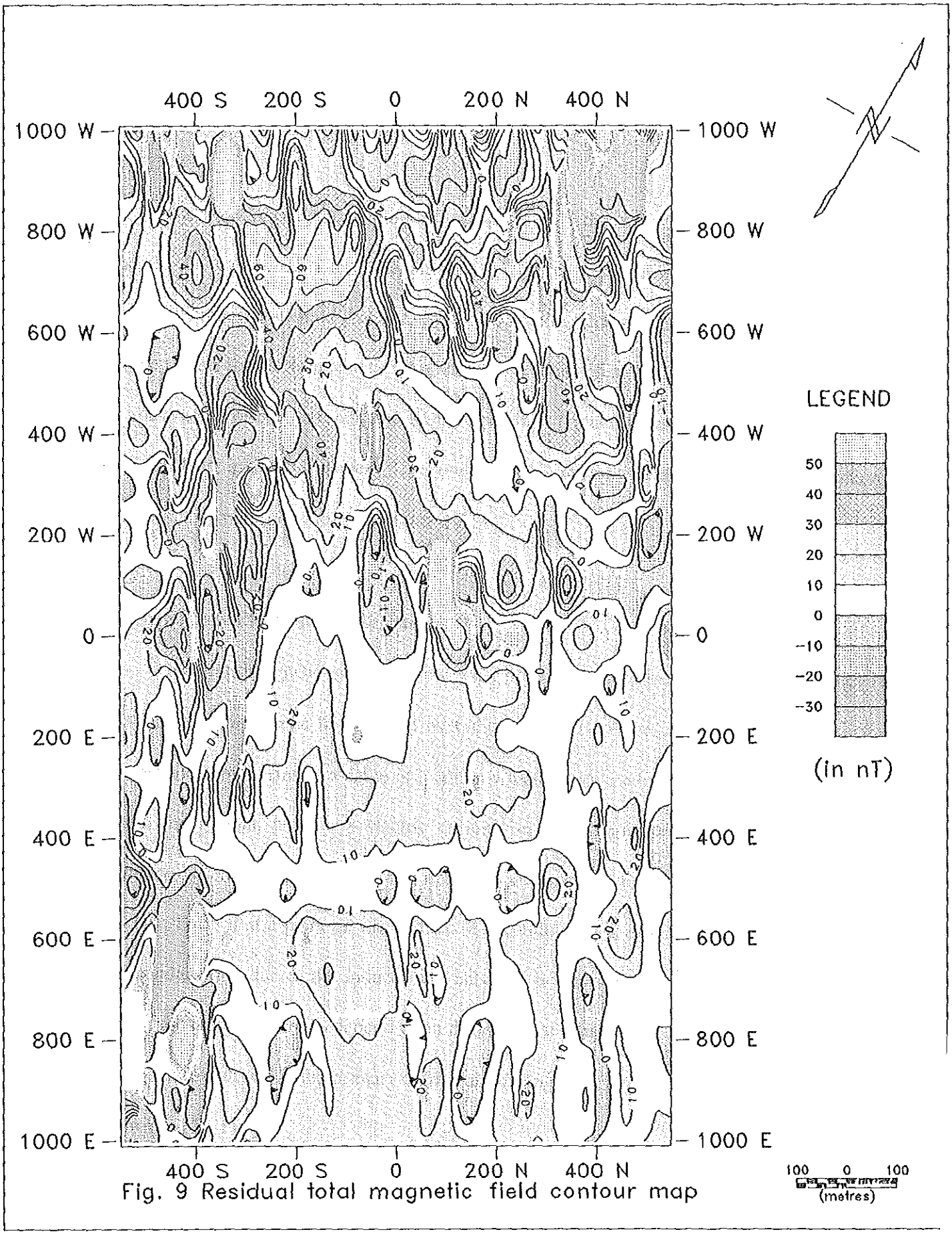

Fig. 9 Residual total magnetic field contour map

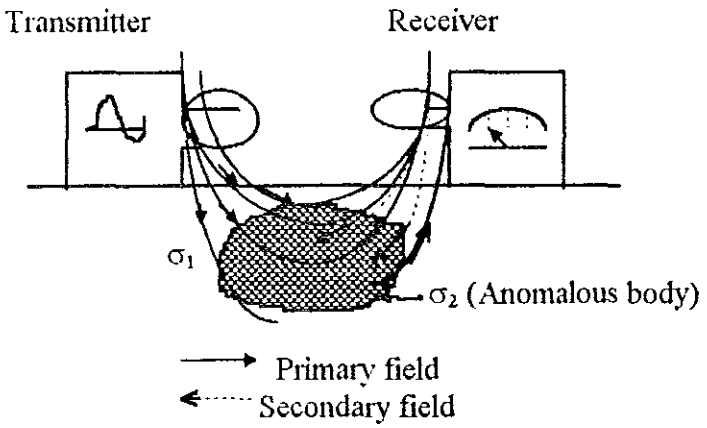

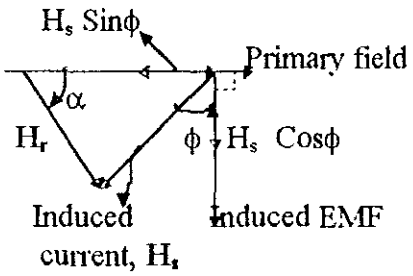

Fig. 10 Schematic diagram of the principle of the EM prospecting. Fig. 11 Phase Diagram

In general $0 \leq \phi \leq \pi/2$; and ϕ is zero for poor conductors and $\pi/2$ for good conductors. At every point in an electromagnetic field there is an electric field (V/m) and a magnetizing force (A/m). The fields are related by Maxwell's equations as

$$\vec{\nabla} x \vec{E} = -\frac{\partial \vec{B}}{\partial t} \text{ - Faraday's Law} \qquad (19)$$

$$\vec{\nabla} x \vec{H} = \vec{J} - \frac{\partial \vec{D}}{\partial t} \text{ - Ampere's Law} \qquad (20)$$

where $\vec{B}$ is the magnetic induction (Wb/m^2). $\vec{H}$ the magnetic field intensity (A/m), $\vec{E}$ the electric field intensity (v/m), $\vec{J}$ the electric current density (A/m^2) and $\vec{D}$ the electric displacement ($coul/m^2$). These field quantities are related to the media parameters as follows:

$$\vec{B} = \mu \vec{H}$$

$$\vec{J} = \sigma \vec{E} \qquad (21)$$

$$\vec{D} = \varepsilon \vec{E}$$

where μ is the magnetic permeability, σ the electric conductivity and ε is the dielectric constant.

In free space

$\varepsilon_0 = 8.85 \times 10^{-12}$ Farads/m; $\sigma_0 = 0$; and $\mu_0 = 4\pi \times 10^{-7}$ henry/m.

Substituting eqns.(21) in Maxwell's eqns. (19) and (20) above, yields

$$\vec{\nabla} x \vec{E} = -\mu \frac{\partial \vec{H}}{\partial t} \tag{22}$$

$$\vec{\nabla} x \vec{H} = \sigma \vec{E} + \varepsilon \frac{\partial \vec{E}}{\partial t} \tag{23}$$

Taking the curl of both sides of eqn. (22) and (23) and substituting in the Maxwell's equations $\vec{\nabla}.\vec{E} = 0$, and $\vec{\nabla}.\vec{B} = 0$, and rearranging, one obtains the general wave equations as

$$\nabla^2 \begin{pmatrix} \vec{E} \\ \vec{H} \end{pmatrix} = \mu\sigma \frac{\partial}{\partial t} \begin{pmatrix} \vec{E} \\ \vec{H} \end{pmatrix} + \mu\varepsilon \frac{\partial^2}{\partial t^2} \begin{pmatrix} \vec{E} \\ \vec{H} \end{pmatrix} \tag{24}$$

For most rock materials $\varepsilon = 9\varepsilon_0$ and $\mu = \mu_0$; and $\sigma = 10^{-3}$ mho/m for good conductors and is about 10^{-4} mho/m for poor conductors (on the average) [21].

At low operating frequencies (the cases considered in electromagnetic prospecting) eqn. (24) can be approximated by

$$\nabla^2 \begin{pmatrix} \vec{E} \\ \vec{H} \end{pmatrix} = 0; \quad \text{for free space} \tag{25}$$

and

$$\nabla^2 \begin{pmatrix} \vec{E} \\ \vec{H} \end{pmatrix} = \mu\sigma \frac{\partial}{\partial t} \begin{pmatrix} \vec{E} \\ \vec{H} \end{pmatrix}; \text{ for earth materials} \tag{26}$$

In practice it is usually the magnetic field that is measured in electromagnetic prospecting [16]. Considering an electromagnetic plane polarized wave in the x-y plane propagating vertically downward in the z-direction into the earth. the magnetic field component is given by

$$H = H_0 e^{-az} e^{i(\omega t - \alpha z)} \tag{27}$$

where H_0 is the amplitude and "a" is the amplitude factor ($a = (\mu\sigma\omega/2)^{1/2}$).

In the absence of subsurface conductors the field at any point oscillates along a definite line and can be represented by a vector of proper magnitude giving the amplitude of the field. The

causative body. Further, on profiles 800W, 900W and 1000W, between stations 155S-95S, weak EM response is detected with both spacings. This EM anomaly has no correlation with the surface geology, but coincides with the high radiometry. Thus, the source of this EM anomaly may be assumed to be a conductive body found in association with pegmatite vein.

On profiles 0 and 100W between stations 300N and 390N a weak EM response is detected by the 100 meters spacing. This result coincided with high radiometry and low magnetic field responses. Graphitic schist is also observed at the field over this zone. Hence, the weak EM anomaly of this zone could be attributed to graphite mineralization of low concentration.

The EM survey has also detected anomalies with moderate amplitude ratio on profiles 100W-800E, between stations 600S and 700S, parallel to the strong EM anomaly detected at the southern margin of the grid. This anomaly has shown up on both transmitter-receiver spacings, except that the anomaly amplitude is relatively diminished for the 50 meters spacing.

On profiles 300W-800W the EM anomaly detected between 200S and 400S has two distinct negative peaks flanked by positive peaks on each side. The two negative peaks correspond to the parallel graphitic lenses separated by quartz-mica schist observed on the surface geological map (Fig. 2), with each directly located below the peaks. The distinct negative peaks are more pronounced on the 50 meters transmitter-receiver spacing (Fig. 13). The distinct anomaly feature is relatively suppressed for the larger transmitter-receiver spacing (Fig. 14) which may be explained interms of the increased spacing that causes the summing up of the effects of both bodies and the introduction of wider resistive area. Each band has an average width of 30-40 meters and a length of 500 meters along the strike.

Similarly, on profiles 600W-1000W between 400S and 600S, the EM response has two distinct peaks for the 50 meters transmitter-receiver spacing. On the other hand, the 100 meters spacing mapped a wide EM response which seems as due to a large anomalous body. However, the

two distinct peaks for the shorter spacing could represent two closely spaced parallel graphitic bodies. The larger spacing has merged the two bodies as if the EM response is from a unified body which may be caused by the increased spacing. To identify the source of this distinct peaks observed on the smaller spacing and the source of the EM anomaly detected between 600S and 700S on the eastern profiles with both spacings geological follow up and application of other geophysical methods are important.

The EM anomalies are equally outlined with both transmitter-receiver spacings, except that the anomaly amplitudes depend on the frequencies and the spacings employed. The anomaly amplitude primarily depend on the conductivity of the target body. Accordingly, the zero EM response detected over the survey area represents the barren rocks hosting the graphitic body. Along the conducting zone of the area, the anomaly amplitude is observed to increase with increasing transmitter-receiver spacing and frequency. Owing to its smaller spacing, the EM survey with the 50 meters transmitter-receiver spacing is clearly seen to display EM response whose anomaly amplitude is relatively diminished. For the same spacing, the anomaly amplitude is observed to increase with increasing frequency. Thus, for both spacings the anomaly amplitude is maximum for the signal frequency 3037.5 Hz. The larger spacing allows better depth of penetration despite its poor resolution. Accordingly, from the effective depth of penetration of the 100 meters spacing, the anomalous body is estimated to extend to a depth of at least 50 meters.

From the asymmetry of the GENIE amplitude ratio curves of both spacings, the anomalous body is suggested to dip to the north.

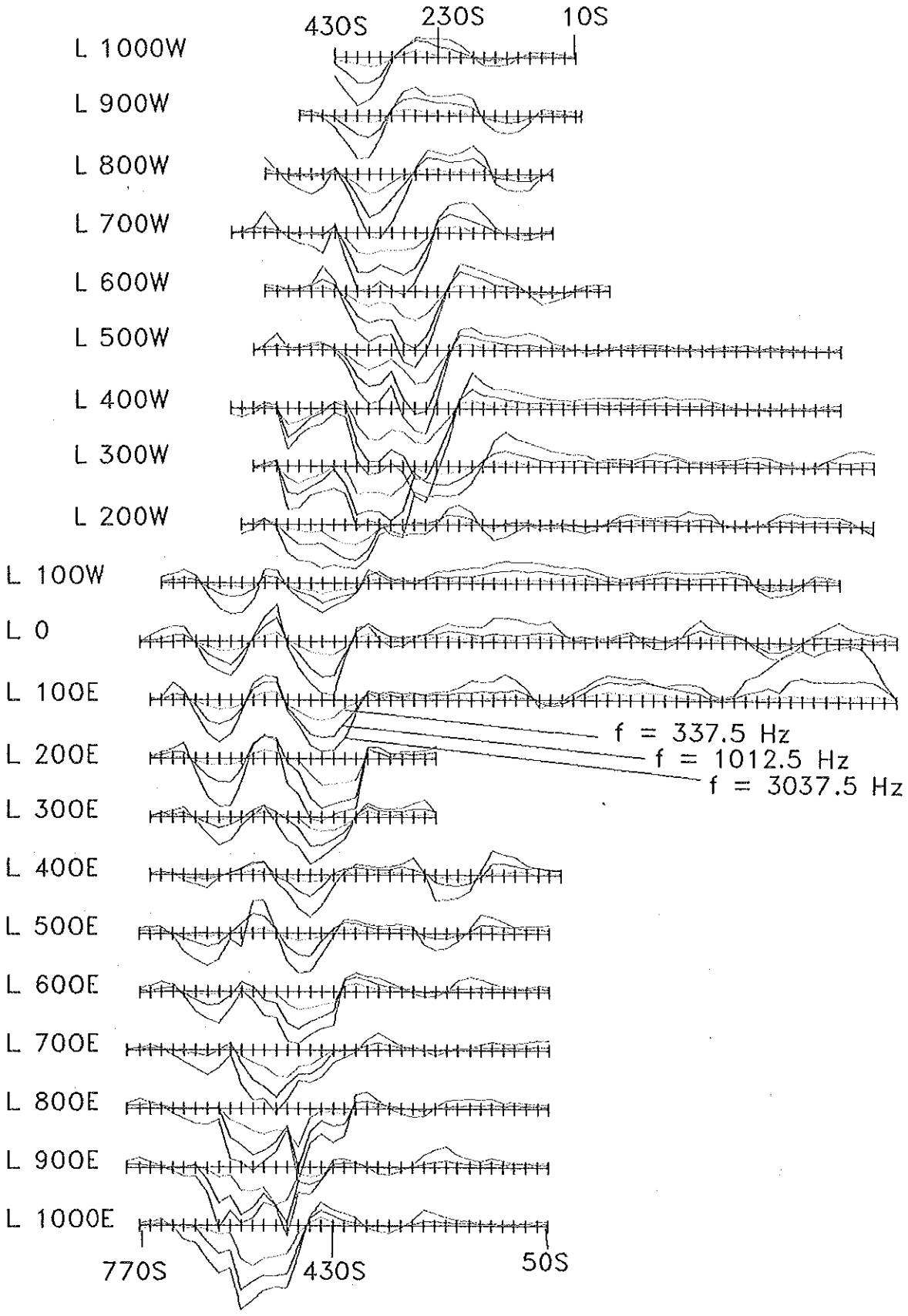

FIG. 14 GENIE amplitude ratio response profiles for Transmitter–Receiver spacing 100 meters

$$\rho_a = 2\pi a \frac{\Delta V}{I} \tag{38}$$

The Schlumberger Array: The Schlumberger array, illustrated in Figure 16(b), is the most widely used configuration. The potential electrode spacing "a" is very small and constant and the current electrode spacing is increased during the measurements, typically at a logarithmic rate. If the potential between the measuring electrodes MN is very small to be measured, the spacing is increased and the measurement is continued with electrode spacing in the series [21].

The apparent resistivity at the center of a Schlumberger array is given by

$$\rho_a = \frac{\pi(S^2 - \frac{a^2}{4})}{a} \frac{\Delta V}{I} \tag{39}$$

where S is half of the current electrode separation (i.e., AB/2).

The Dipole-Dipole Array: In this arrangement the current electrodes are well separated from the potential electrodes (Fig. 16 C). The dipole-dipole arrangement is commonly used because of its deep penetration and less electrode polarization problem [17].

If the separations "a" and "b" are equal and the distance between the centers of the respective pairs is (n−1)a, the apparent resistivity determined by this arrangement is given by

$$\rho_a = \pi n a (n+1)(n+2) \frac{\Delta V}{I} \tag{40}$$

where n = 1, 2, 3, ...

Pole-Dipole array: If one of the current electrodes, say electrode B, of the dipole-dipole arrangement is assumed to be at a great distance from the measurement location, the configuration reduces to a different arrangement known as pole-dipole array illustrated in Figure 16 (d). For this arrangement equation (37) reduces to

$$\rho_a = 2\pi n a (n+1) \frac{\Delta V}{I} \tag{41}$$

where n = 1, 2, 3, ...

The Central Gradient Array: The central gradient array (Fig. 16 (e)) is a special case of the Schlumberger arrangement with current electrodes fixed at positions outside the survey area while the potential electrode pair, MN, is moved along the profiles within the limits of the survey area. For this configuration the apparent resistivity is given by

$$\rho_a = K\frac{\Delta V}{I} \qquad (42)$$

where $K = \dfrac{2\pi}{\dfrac{1}{r_{AM}} - \dfrac{1}{r_{BM}} - \dfrac{1}{r_{AN}} + \dfrac{1}{r_{BN}}}$

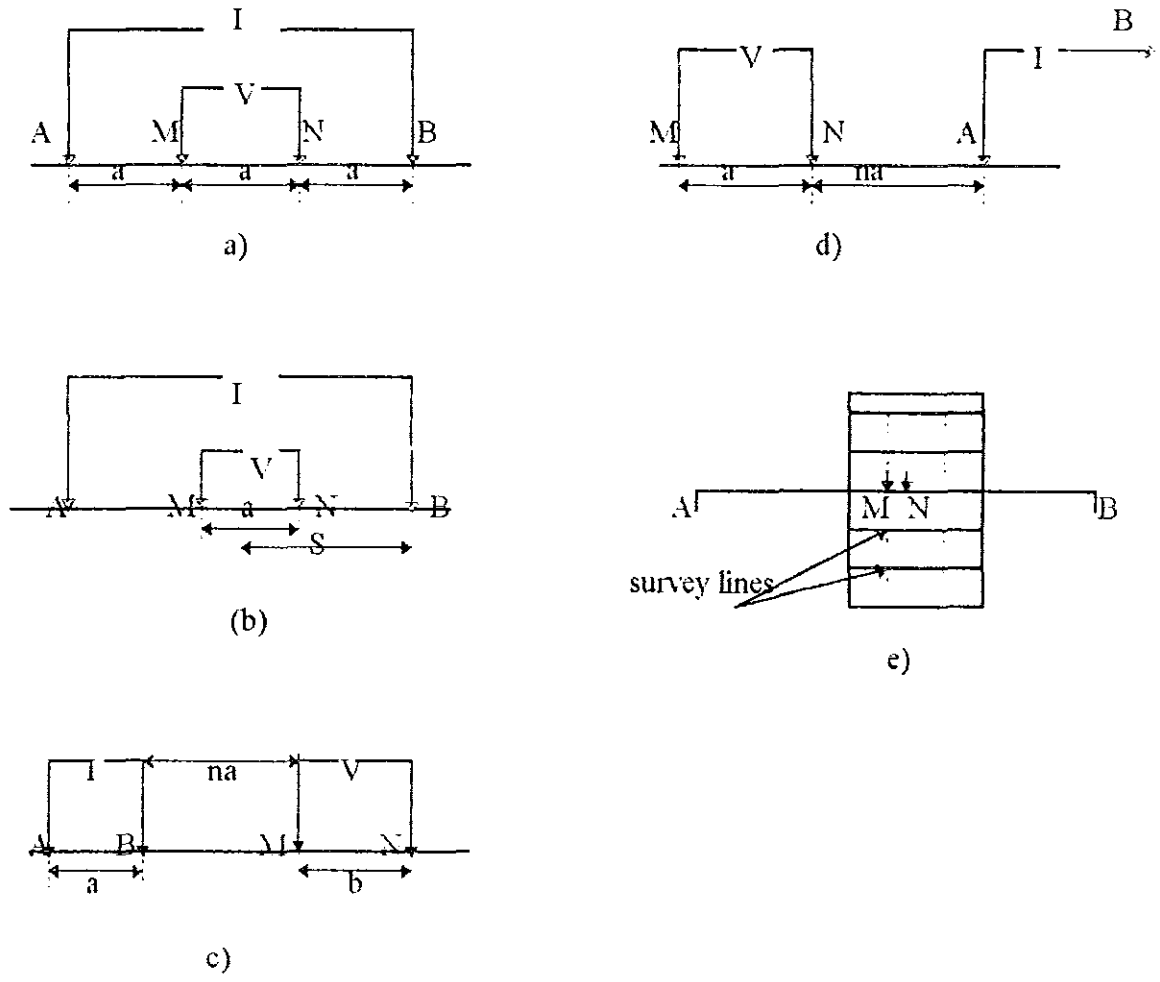

Fig. 16 Collinear electrode configurations in common use:
a) Wenner array b) Schlumberger array c) Dipole - Dipole or Axial array
d) Pole - Dipole array e) Central Gradient array.

5.1.4 Field Procedures

Resistivity surveys are carried out using one or both of the two distinct techniques known as electrical sounding and electrical profiling (mapping). These are more or less complementary to each other but electrical mapping is the more important in ore prospecting [17].

Electrical Sounding: electrical sounding is carried out by fixing the center of the electrical spread while the separation of electrodes is progressively increased. As the current electrode separation is increased, the electric potential distribution on the surface will be affected relatively more by deep-lying inhomogeneities within the earth.

In sounding with the Wenner array (Fig. 16 (a)), the separation "a" is increased in steps by moving each of the four electrodes outwards from the center, typically with set of separations "a" = 2, 6, 18, 54,... n, etc. In the Schlumberger sounding method, the potential probes are fixed at the center of the AB while the current electrodes are moved symmetrically outwards in steps. In the dipole-dipole and pole-dipole, the value of "n" is increased for better depth penetration. The sounding method has an advantage in exploration objectives requiring depth control which can only be achieved through expanding the geometry of the electrode configuration [17,5].

Electrical Profiling: The Electric profiling (mapping) technique is of considerable importance in mineral prospecting. Results of electrical profiling in mineral exploration include location of vertical/subvertical structures which are likely to be identified with large resistivity contrasts, such as faults, contacts, dikes, shear zones and steeply dipping veins and three-dimensional bodies such as massive sulphides [5]. Such lateral variations in the ground resistivity anomaly can be successfully detected by continuous profiling with a fixed configuration. The electrical profiling is carried out using any of the electrode configurations shown in Fig. 16 with the electrode spacing fixed and the

array moved laterally along the profiles. The computed apparent resistivity is plotted at the mid-point of the potential electrodes. Any ore body having anomalous conductivity and which is shallower than the depth of the maximum effective penetration should show up as an anomaly on the resulting map [17,5].

In the Wenner profiling, the four electrodes with fixed spacing are moved along the line of measurement. Each electrode is then advanced through the same distance. In the case of the gradient survey, the current electrodes are kept fixed, and the length of the profile to be surveyed makes up 1/3 to 1/4 of the separation of the current electrodes. The potential probes with a small mutual separation are then moved along the line of measurement [17].

In the present study, the IP Resistivity surveys were carried out on the same profiles as in the previous methods, using the Central Gradient and the Pole-Dipole arrays illustrated in fig. 16 (d) and (e). For the purpose, a TSQ-3 transmitter, powered by an 8 HP Briggs and Stratton motor generator, and the digital IPR-10A time-domain receiver were used. In addition, non-polarizing porous pots as potential electrodes, stainless steel stakes as current electrodes, steel wires for connecting current electrodes and copper wires for connecting potential electrodes were used. With these set, the third slice of the IP decay curve along with the primary voltage V_p and the transmitter current I were recorded at every 20 meters station interval. Throughout the survey, the transmitter and receiver duration was 2 seconds.

During measurements with the Central Gradient array, the current electrodes (A and B), were staked at 740N and 740S. The potential electrodes (M and N) with a spacing of 20 meters were then moved along the profiles extending between 540N and 540S to measure potential fields. The center point of profile between electrodes M and N was defined as the point of measurement.

The Pole-Dipole array with spacing, "a", of 20 meters (Fig. 16 (d)) was used on 10 profiles. The measurements were taken at every 20 meters station interval by increasing the spacing

between the current and potential electrodes from 1 to 6 times the dipole length. The results are plotted at the midpoint of current electrode A and potential electrode M [21].

5.1.5 Data Processing, Presentation and Interpretation

Data Processing and Presentation: Eqns. (41) and (42) were used for computing apparent resistivities for the central gradient and pole-dipole arrays, respectively. Both the gradient and pole-dipole survey data were gridded at 5 units cell size and then contoured using the "geosoft" mapping and processing system. The contour and pseudosection maps are shown in Figs. 17, 18 and 19. Because of the large difference between the least and highest resistivity values, the contour maps for both arrays were prepared at a contour interval of 0.3 in a logarithmic scale.

Data Interpretation:

a) Central Gradient Array

From the apparent resistivity contour map shown in Fig. 17, two major anomalous zones of low apparent resistivities (less than 10 Ohm-meter) are observed. The first anomalous zone extends from 1000W to 900E along the southern margin of the survey grid. Between lines 500W-1000W and 100W-900E, this zone has an average width of 70 meters whereas between lines 500W-100W its width increases to 200-250 meters. This thin and elongated anomalous zone lies along 360S in the western and along 500S in the eastern grid and coincides with the strong radiometry and electromagnetic and weak magnetic (ΔT) responses. The low resistivity values detected within this zone are attributed to graphite mineralization. During the field survey, surface exposures of graphitic bodies were encountered following this geophysical anomalous zone. This zone opens to the west indicating the possible extension of the mineralized body beyond the surveyed grid, whereas to the east it closes around 900E. The relatively greater anomaly width

detected between 100W and 500W could be due to intercalation of the graphite schist into the host rock and its dipping effect.

The second low resistivity zone (less than 10 ohm-m) is relatively small in its areal distribution and is detected at the central part of the grid between 100E/0 and 200W/300N. By the same analogy, the source of this anomalous zone is attributed to the graphite mineralization. Other patches of anomalies with low resistivity (less than 10 Ohm-m) are mapped parallel to the main anomalous zone at 300E/200N and 500E/500N which are also assumed to have similar causative body as the main zone.

The high apparent resistivity zone (greater than 1000 Ohm-meter) delineated between 600W/0 and 1000W/550S coincides with enhanced radiometry total count measurements. Within this zone occurrences of pegmatite and quartz veins are encountered. Hence, the high apparent resistivity values could be associated with these formations and fresh bed rocks. The enhanced resistivity values (above 1000 Ohm-m) detected at the eastern margin of the grid do not correlate either with the radiometry or magnetic survey results. Probably these values have resulted from the compacted and fresh bed rocks.

The moderate apparent resistivities (10-1000 Ohm-meters) measured over the majority of the survey grid may represent the mafic-ultramafic rocks such as talc-tremolite, talc-tremolite-actinolite and amphibolite schists.

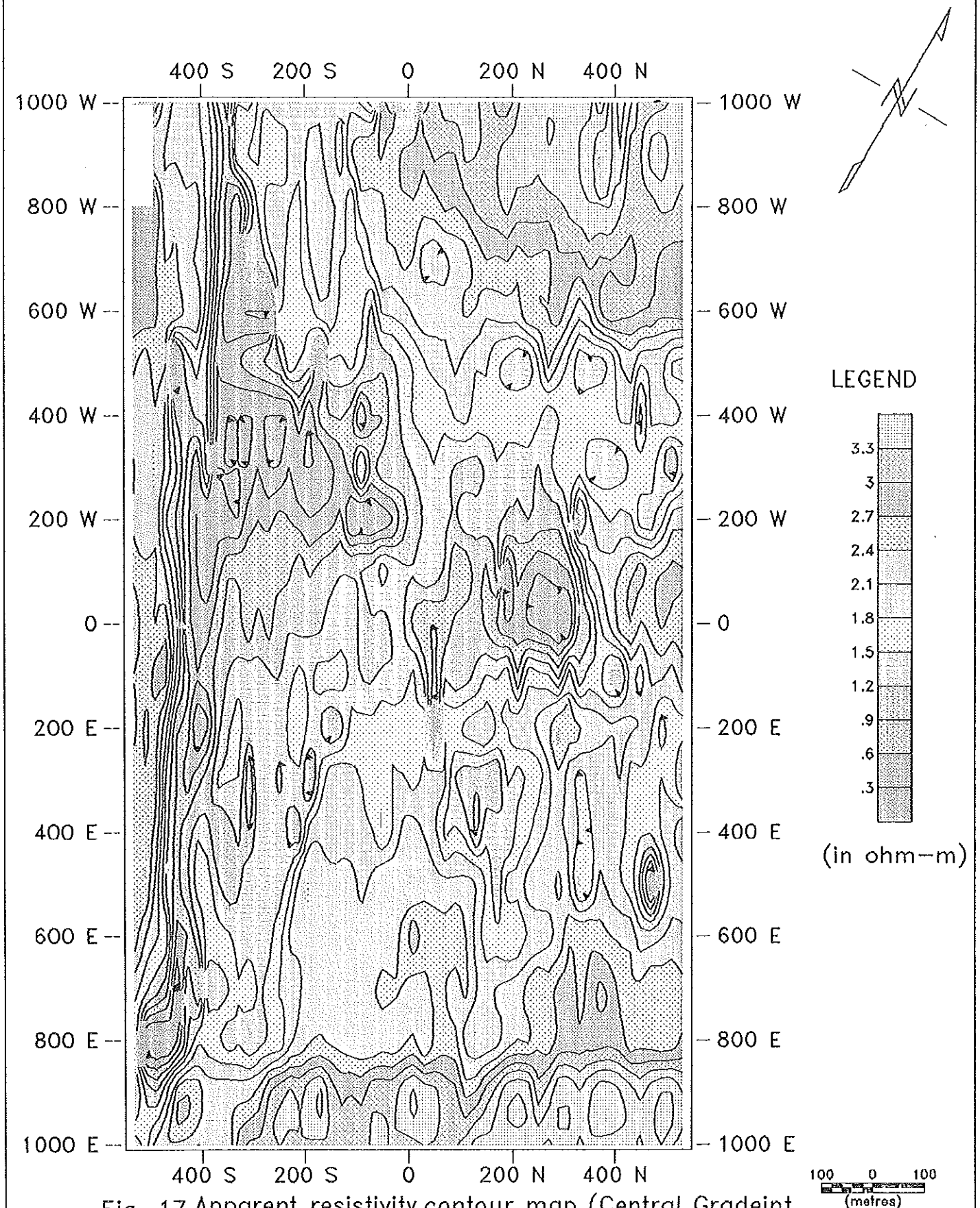

Fig. 17 Apparent resistivity contour map (Central Gradeint array) (C.I = .3, Logarithmic)

b) Pole-Dipole array

From the apparent resistivity pseudosection map shown in Fig. 18, resistivity lows (less than 10 Ohm-meters) are observed along 400S in all sections. The apparent resistivity plan map for the maximum pole-dipole spacing (i.e., for n=6) (Fig. 19) has shown a similar anomaly trend and amplitude as the gradient apparent resistivity contour map (Fig. 17) which indicates the possible depth extension of the graphite mineralization. Accordingly, the anomalous body appears to be extending to a depth of not less than 60 meters i.e., within the limit of effective depth of penetration of the pole-dipole array (n=6).

Other minor anomalies on profiles 200 W, 100 W, 0, 100 E and 200E are also observed whose amplitude increases at depth. These patches of anomalies could be explained to be due to the downward extensions of the central anomaly observed on Fig. 17 between 200E and 200W. The moderate apparent resistivities (10-1000 Ohm-meters) representing the mafic-ultramafic rocks and the high resistivities (>1000 Ohm-meters) at the northwest of the grid which were assumed to be due to the fresh bed rock, are also observed at depth with similar trend as was shown on the gradient resistivity map.

Looking at the trend of the contour lines of the pseudosections, the anomalous body appears uniformly dipping to the north which also agrees with the EM survey result.

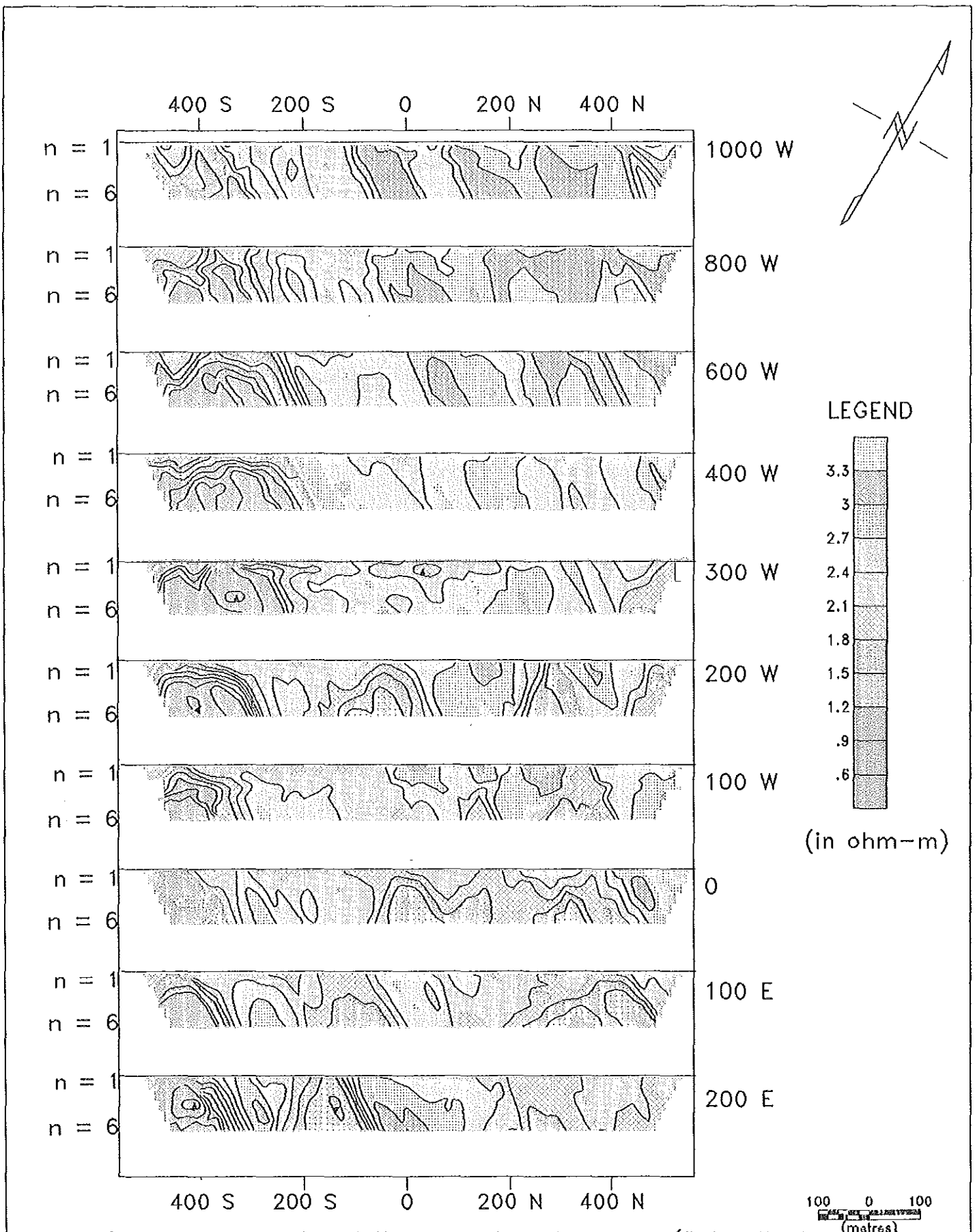

Fig. 18 Apparent resistivity pseudosection map (Pole-dipole array)
(C.I = .3, Logarithmic scale)

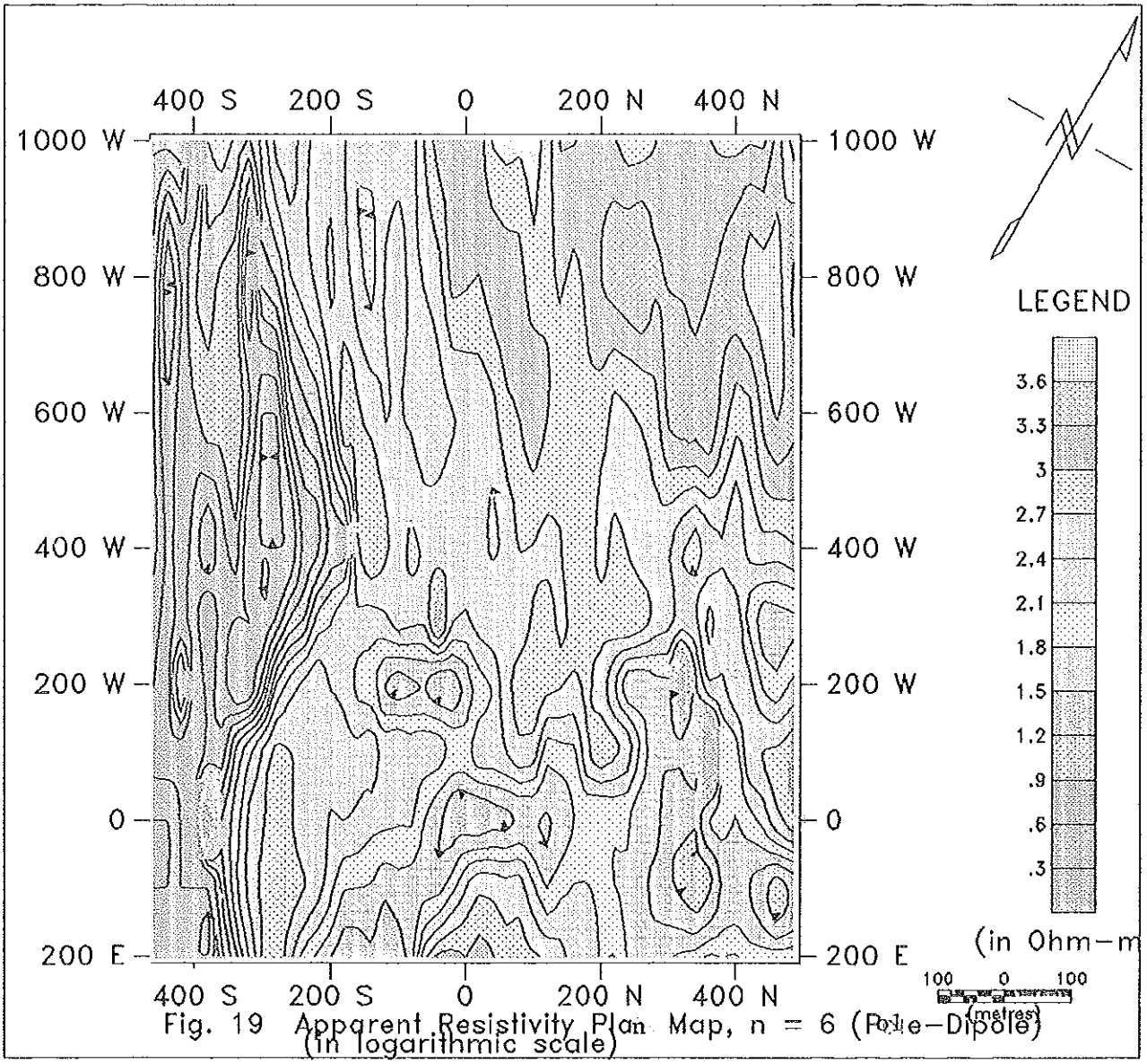

Fig. 19 Apparent Resistivity Plan Map, n = 6 (Pole-Dipole)
(in logarithmic scale)

5.2 Induced Polarization Method

The method of Induced Polarization (IP) has been successfully used in base metal search, particularly in the search for low grade deposits. In areas of disseminated mineralization, such as porphyry coppers where the resistivity anomaly could be considered non-existent, the IP method has been found to show a good response [17]. It is also used for exploration of oxides, sulphides, graphite and others [20].

Qualitative interpretation of the IP data from the profiles yields information about the location, lateral extent and the depth of anomalies. These quantities are estimated from the characteristics of the profile plots such as sharpness, symmetry, and amplitude above background. By traversing with several different electrode separations, it is often possible to resolve multiple anomalies and gain some idea of their depth extent. The method of induced polarization fairly gives good depth estimate and has a considerable depth of penetration despite the ambiguity it presents as to the location of the target, undesirable effects of near surface variations and slow field operations [21].

5.2.1 Sources of the Induced Polarization

When current flows through the ground, some energy storage takes place in the form of mechanical, electrical and chemical energy. The chemical energy is by far the most dominant energy storage mechanism in the process and is due to variations in the mobility of ions in fluids throughout the rock structure and variations between the ionic and electronic conductivity where metallic minerals are present. The first effect is known as membrane polarization (electrolytic). The latter, which is more pronounced, is known as electrode polarization.

When the external current/voltage is applied to the ground, the electrochemical exchange creates a voltage which opposes the current flow through the material. When this externally applied

current is turned off, the electrochemical voltage at the interfaces is dissipated, but not instantaneously (Fig. 20). This decaying voltage can be measured for a certain time after the current is switched off [5].

The membrane polarization constitutes the background or the so-called normal IP effect which has to be compensated during IP measurements [21].

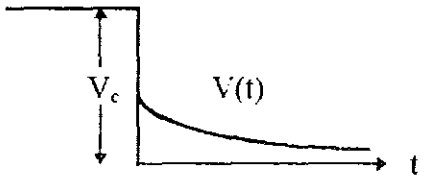

Fig. 20 IP decay (over voltage) curve.

Electrode Polarization: Minerals which are electronic conductors exhibit electrode polarization. Since the velocity of current flow in metals is much higher than in the electrolyte, the piling up of ions is maintained by the external voltage. When the current is interrupted, the residual voltage decays as the ions diffuse back to their original equilibrium state. This effect is observed in oxides, sulphides, metals, graphite and graphite schists [20,21].

The magnitude of polarization is higher for disseminated minerals than for massive ones because it is a surface phenomenon. Thus, one would expect high IP effect in a disseminated sulphide occurring in compacted rocks than in the porous ones. Further, the magnitude depends on the external current source and mineral concentration. For a particular concentration it decreases with increasing porosity [21].

5.2.2 Induced Polarization Measurements

The field procedures for induced polarization (IP) surveys are similar to that of the resistivity methods described in section (5.1.4). The different configurations illustrated in Fig. (16), for the resistivity methods also apply to induced polarization measurements. The IP measurements can be done either in time domain or in frequency domain.

5.2.2.1 Time Domain Measurements

a) IP percent

The ratio of the residual voltage V(t), in millivolt, existing at a time t after the current is cutoff to the steady voltage V_c, in volt, during the current flow interval gives the simplest way to measure IP effect in time domain (Fig. 20). When both quantities are expressed in millivolts, IP percent is defined as

$$IP\% = \frac{V(t)}{V_c} x100\% \qquad (43)$$

b) Decay time integral

IP sets generally measure area under decay curves (Fig. 20) over a definite time interval (say, between time t_1 and t_2). Thus, the time integral is given by

$$\text{Decay time integral} = \int_{t_1}^{t_2} V(t)dt \qquad (44)$$

where V(t) is the residual voltage in millivolts

c) Chargeability

The chargeability (M) measurement is widely used in time domain IP measurements. It is the extension of the decay time integral and is defined as

$$M = \frac{1}{V_c}\int_{t_1}^{t_2} V(t)dt \qquad (45)$$

where V_c is the steady voltage that exists before interrupting the current. Chargeability(M) is given in millisecond when both V(t) and V_c are expressed in the same unit.

5.2.2.2 Frequency Domain Measurements

a) Frequency effect

If an alternating current is made to flow through the ground, the over voltage observed at the metallic surface will decrease with increasing frequency because the build up of the opposing voltage to its full value requires a longer time than the period between changes in direction of the applied current [20]. This phenomenon makes possible the measurement of apparent resistivities at two or more frequencies. If apparent resistivities ρ_{DC} and ρ_{AC} are the measured values at low and high frequencies, respectively, the frequency effect (f_e) is given by

$$f_e = \frac{\rho_{DC} - \rho_{AC}}{\rho_{AC}} \qquad (46)$$

and the percent frequency effect (PFE) is expressed as

$$PFE = \frac{\rho_{DC} - \rho_{AC}}{\rho_{AC}} X100\% \qquad (47)$$

In practice, measurements are made at two or more frequencies in the range of 0.1 Hz to 10 Hz; ρ_{DC} is greater than ρ_{AC} being the value taken at the lowest frequency [21].

b) Metal Factor

Since the IP effect varies with effective resistivity of the host rock, i.e., the type of electrolyte, temperature, pore size, etc., the metal factor parameter (MF) corrects to some extent for these variables. It is expressed as

$$MF = 2\pi 10^5 \frac{\rho_{AC} - \rho_{DC}}{\rho_{AC}\rho_{DC}} \qquad (48)$$

When apparent resistivity is in ohm meter, metal factor (MF) is expressed in mho per meter.

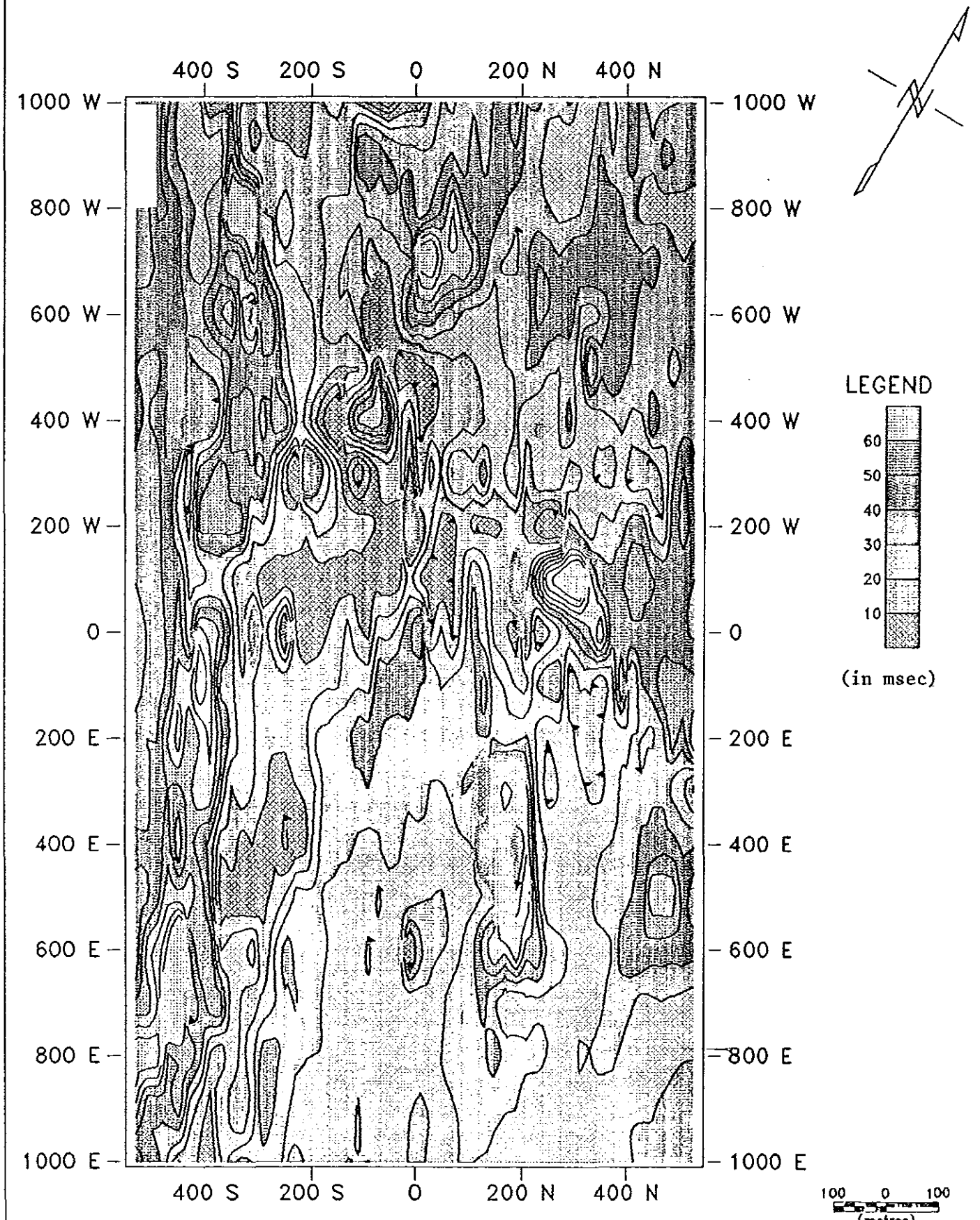

Fig. 21 Chargeability contour mcp (Central Gradient array)(C.I = 10 ms

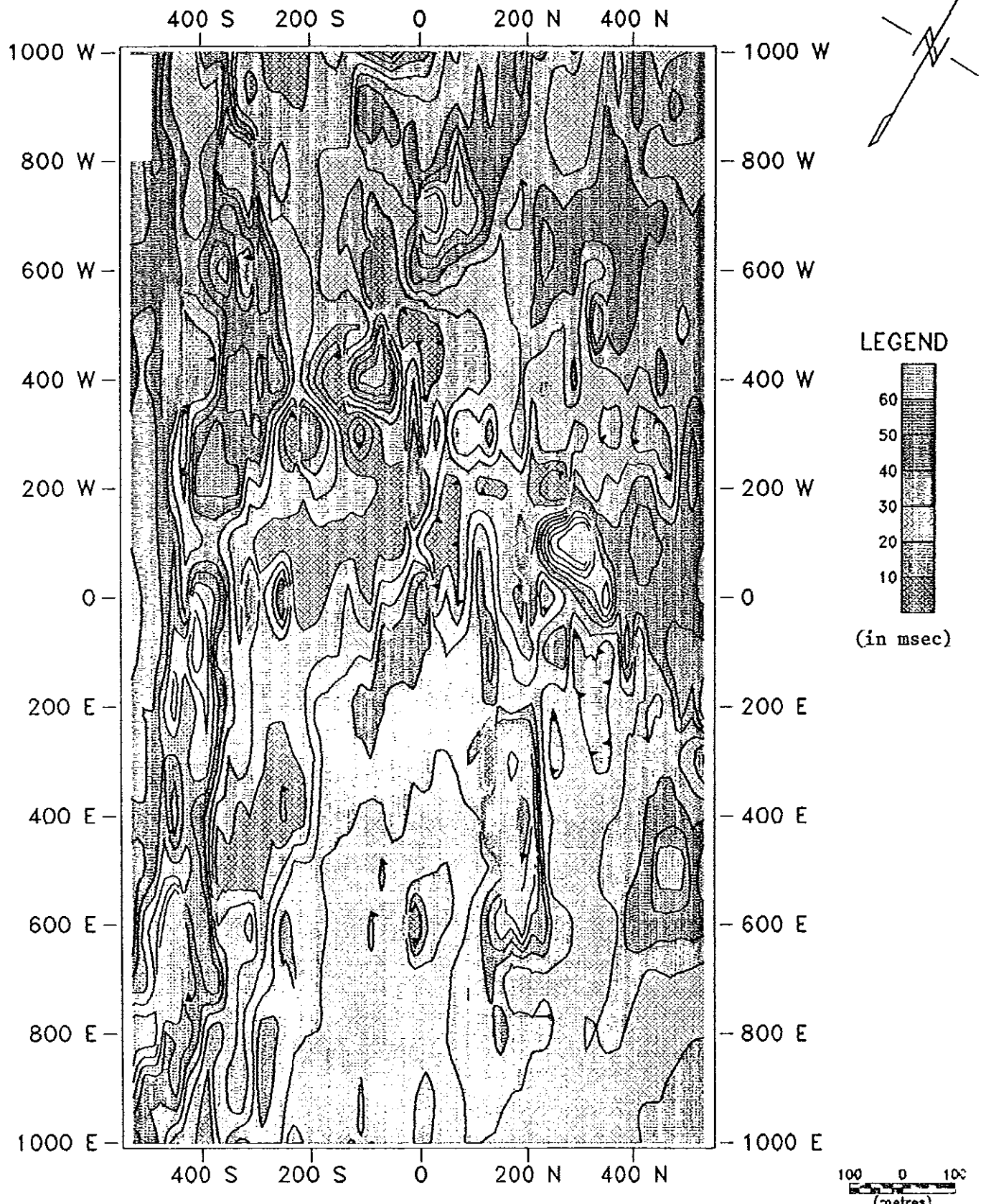

Fig. 21 Chargeability contour map (Central Gradient array) (C.I = 10 ms

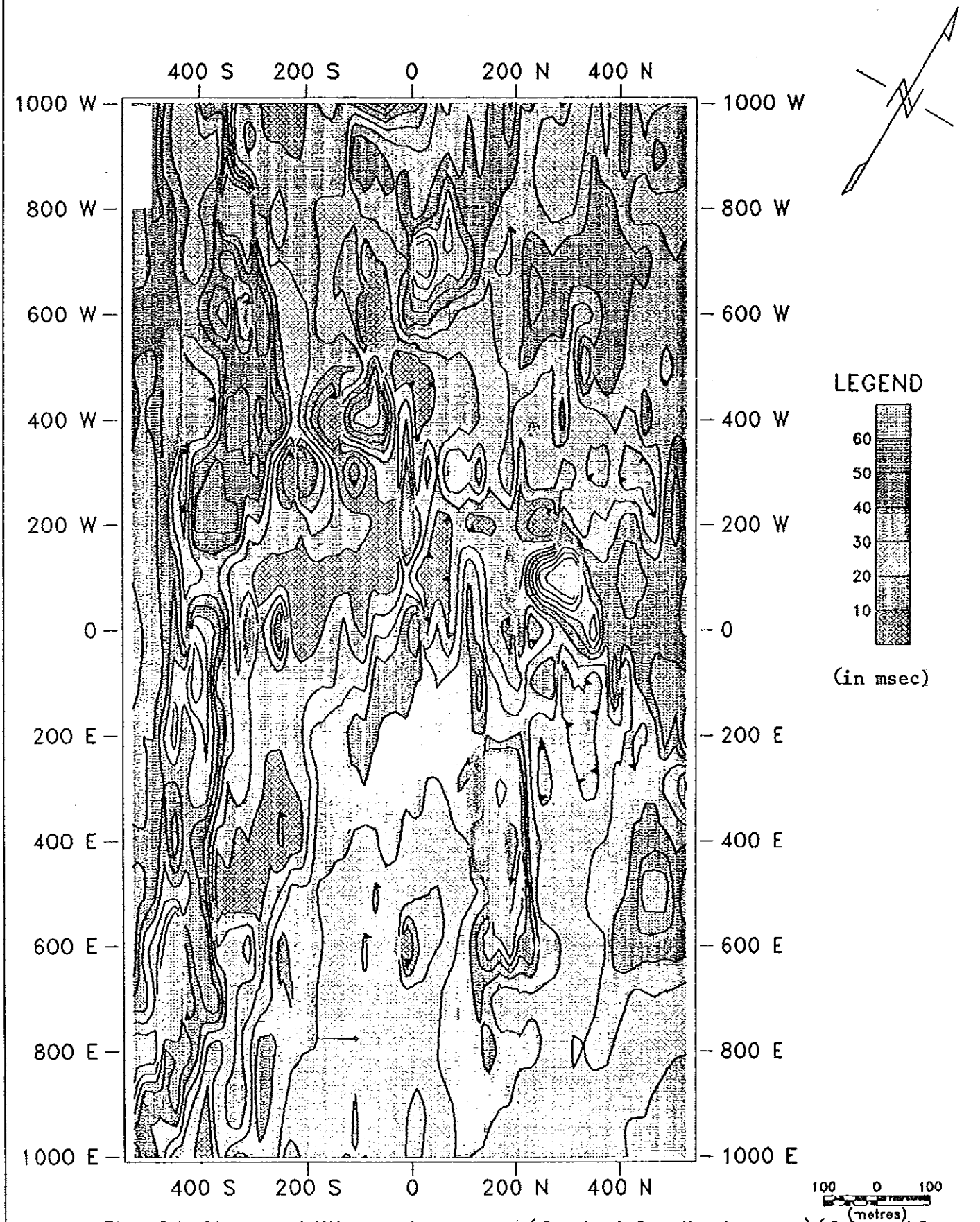

Fig. 21 Chargeability contour map (Central Gradient array)(C.I = 10 ms

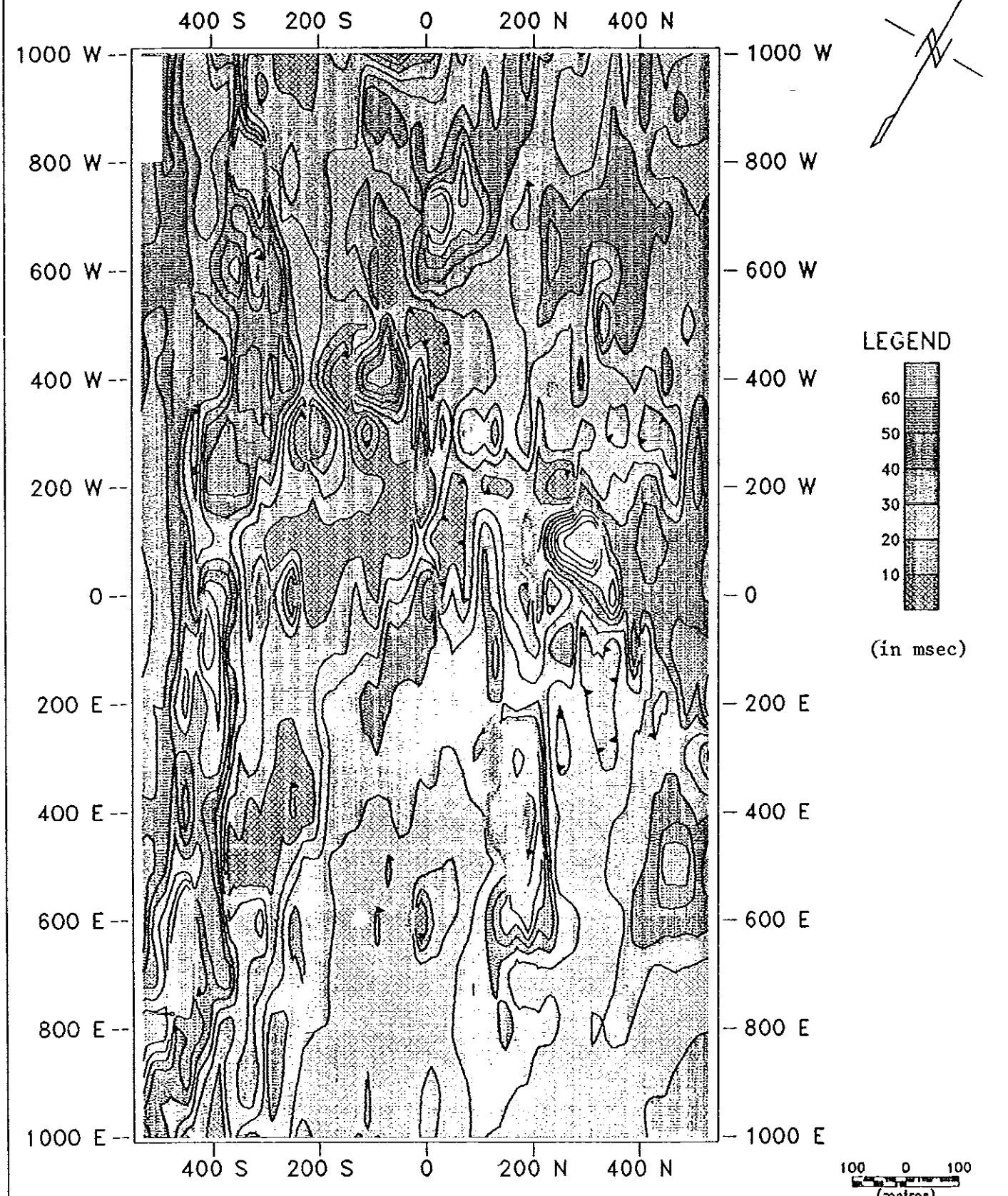

Fig. 21 Chargeability contour map (Central Gradient array)(C.I = 10 ms

The north-west portion of the grid which was identified by high radiometry and high apparent resistivity values has shown moderate to high chargeability response (40-70 msec). This zone has no clear correlation with the surface geology. However, the high chargeability is assumed to be due to disseminated graphite mineralization found in association with the pegmatite veins and the host rock.

The low chargeability response (less than 30 msec) is attributed to the barren host rocks represented by the mafic-ultramafic rocks such as talc-tremolite, talc-tremolite-actinolite and amphibolite schists.

b) Pole-Dipole array

On the IP pseudosection map (Fig. 22), chargeability highs (greater than 50 msec) are clearly detected between stations 300S and 500S in all sections. These high IP values fairly correspond to the low resistivity zone shown in Fig. 18. The anomalies appear to extend to a considerable depth within the limit of the effective depth of penetration of the pole-dipole array with dipole spacing of n=6 (approximated to be 60 meters). However, on profile 300W the intensity of IP values show a significant drop with depth indicating that the causative body is limited to shallow depth. The pole-dipole chargeability plan map for n = 6 (Fig. 23) has shown similar anomaly trend and amplitude as that of the gradient chargeability (Fig. 21), and this indicates the possible presence of graphite mineralization at depth.

On some profiles (400W, 300W, 200W, 0, and 200E), along the main anomalous zone, the anomaly is observed on n = 1 which reveals the possible presence of outcropped and/or shallow anomalous bodies. This result is in good agreement with the encountered graphite surface exposures in the field and, in some cases, with similar bodies exposed by trenching at depths of 0.5 to 1 meter. On the other hand, on lines 100W and 800W no anomalous signature was noted on the n = 1 level. This may indicate that the causative body is not exposed on the ground surface

Other patches of anomalies at depth are also observed on the chargeability pseudosection map with fair overlapping with resistivity result (Fig. 18). The high chargeability values detected at 100W/0-250N, 0/0-300N and 100E/200-300N coincide with the resistivity lows, and it could be due to the downward continuation of the surface anomaly observed at central part of the grid. Similarly, the anomaly detected at 1000W/0-300N and 800W/0-200N may be the depth extension of the surface anomaly observed at the northwest of the grid which is complementing the assumption made on the possible presence of disseminated graphite mineralization in this zone.

The chargeability pseudosections have indicated anomalous body dipping to the north, which agrees with the resistivity and EM survey results and the field observation.

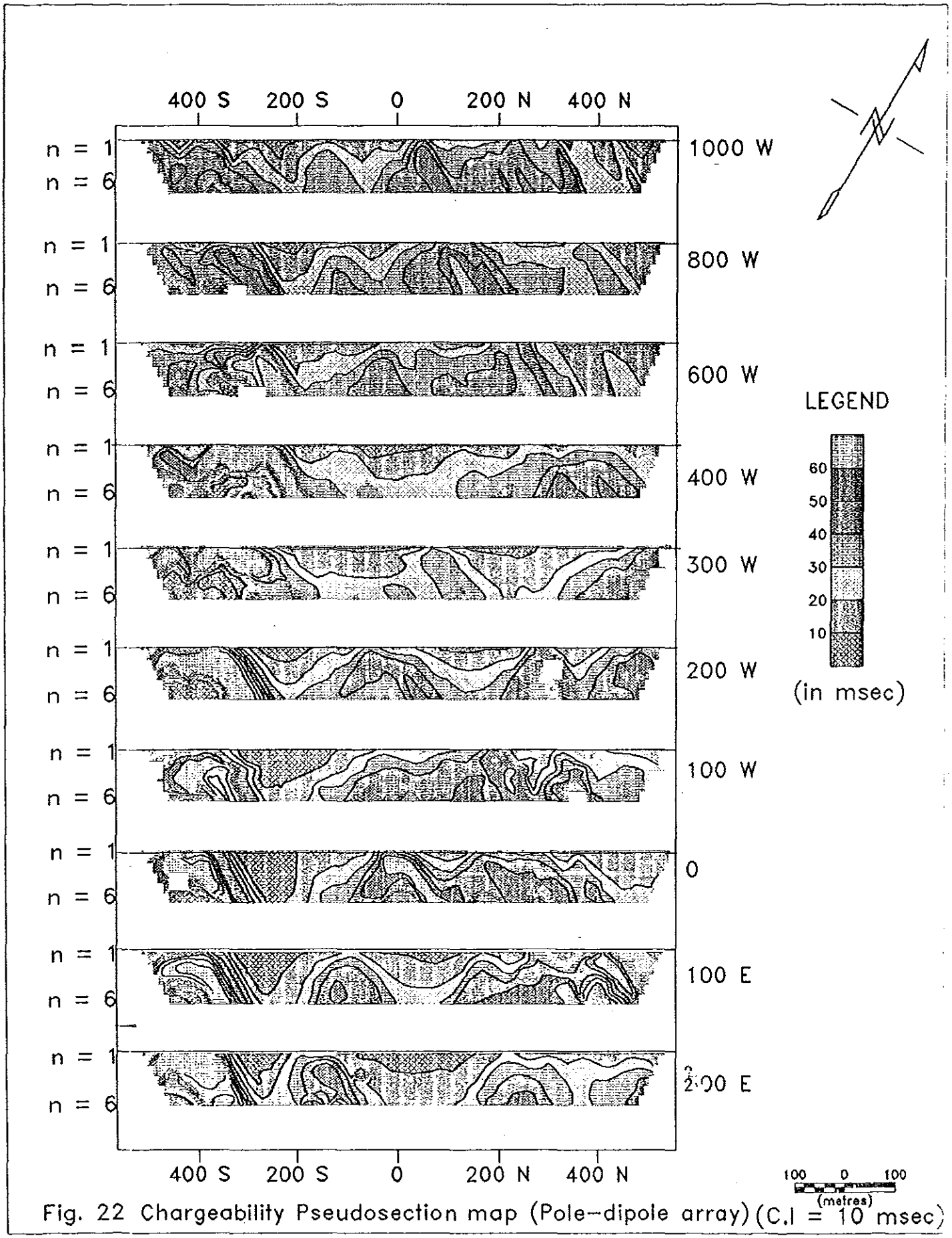

Fig. 22 Chargeability Pseudosection map (Pole–dipole array) (C.I = 10 msec)

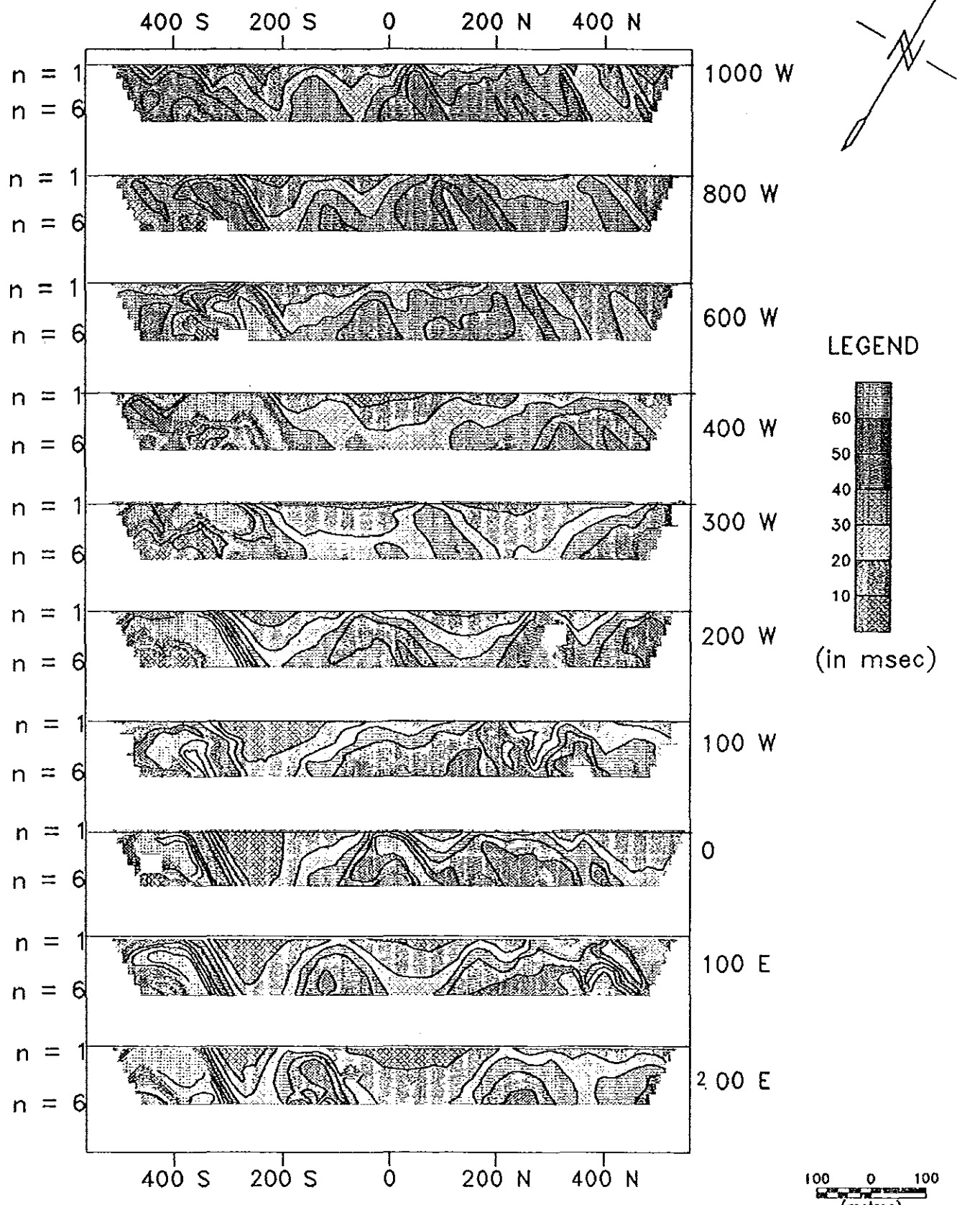

Fig. 22 Chargeability Pseudosection map (Pole–dipole array) (C.I = 10 msec

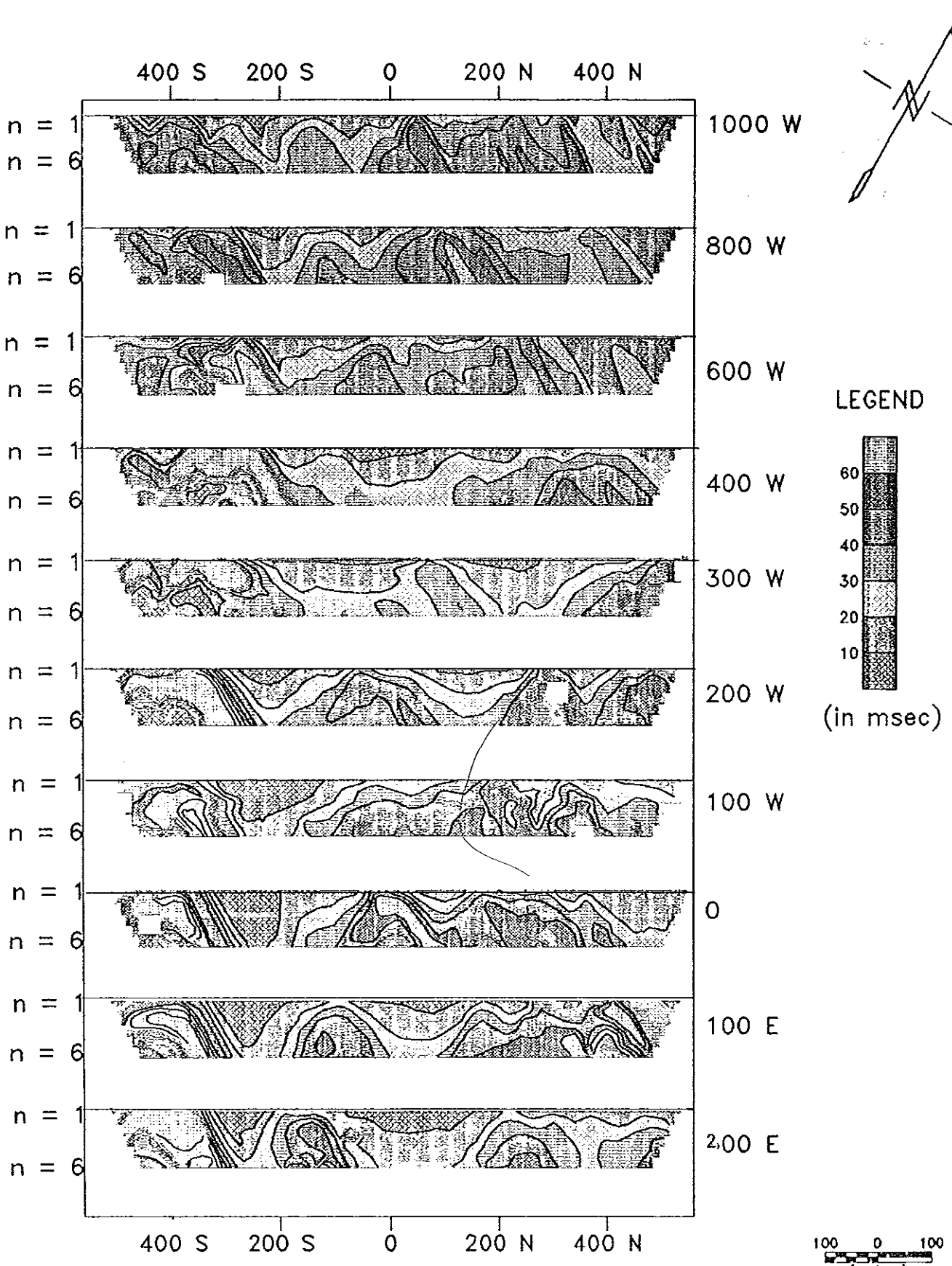

Fig. 22 Chargeability Pseudosection map (Pole–dipole array) (C.I = 10 msec)

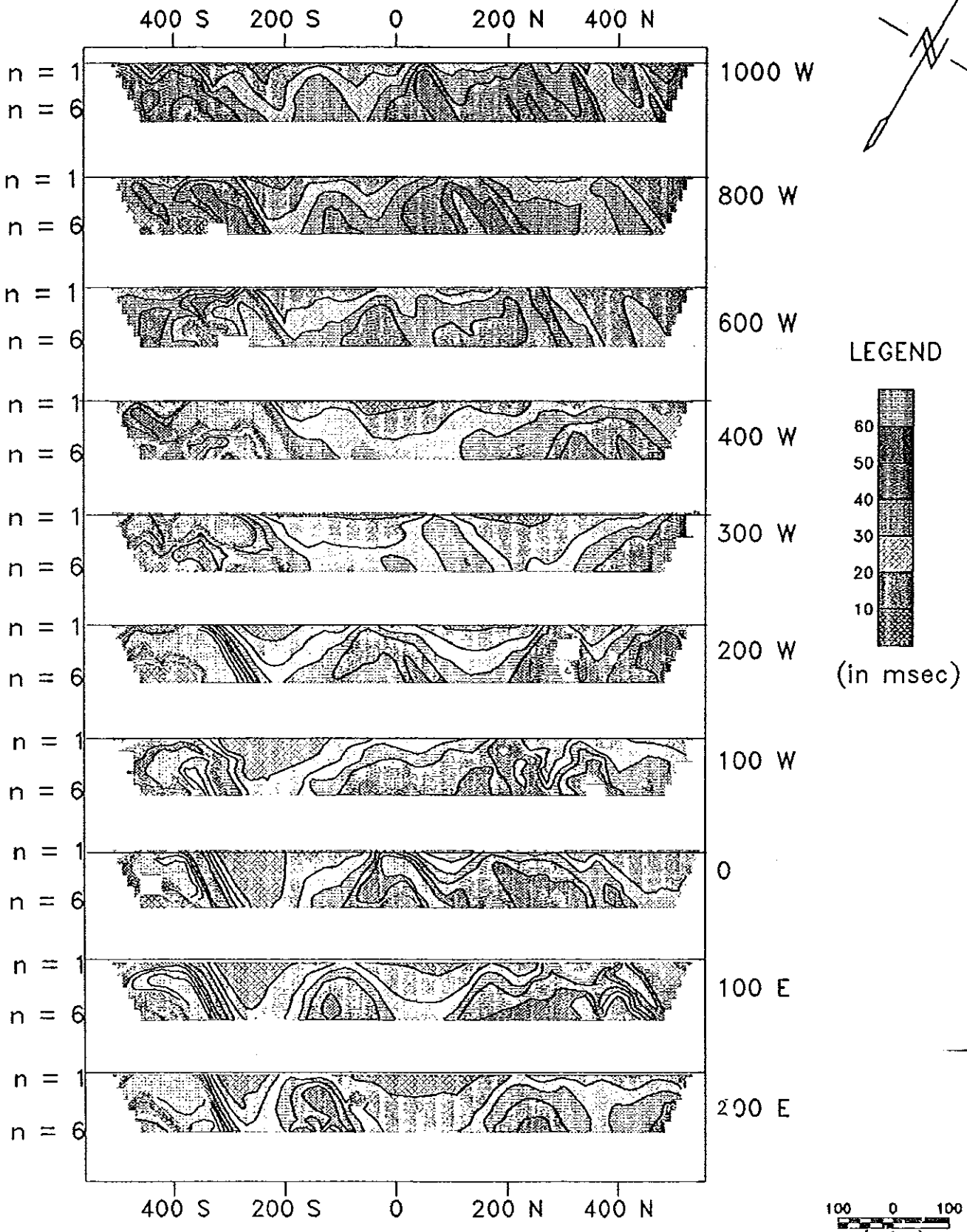

Fig. 22 Chargeability Pseudosection map (Pole–dipole array) (C.I = 10 msec)

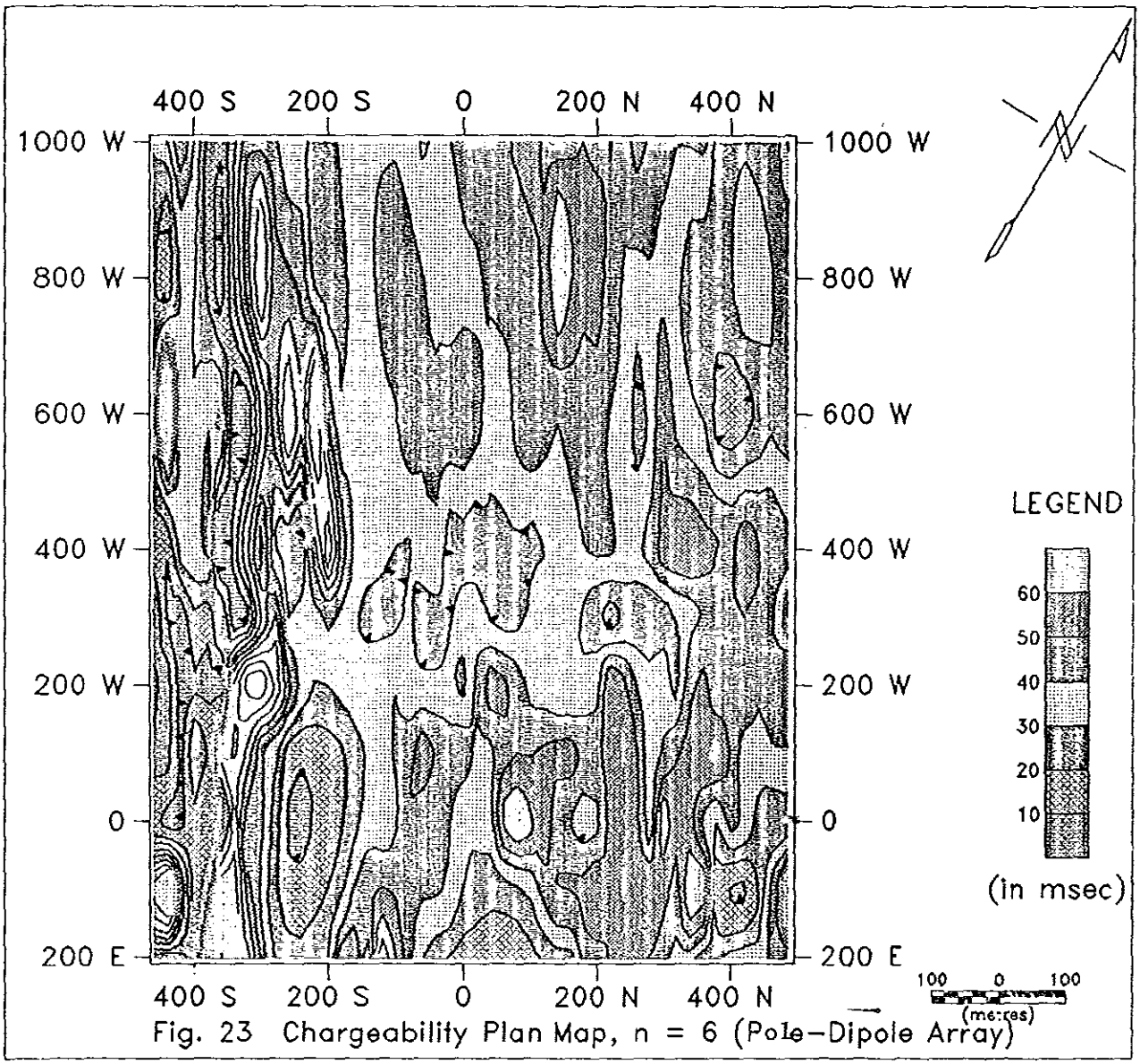

Fig. 23 Chargeability Plan Map, n = 6 (Pole–Dipole Array)

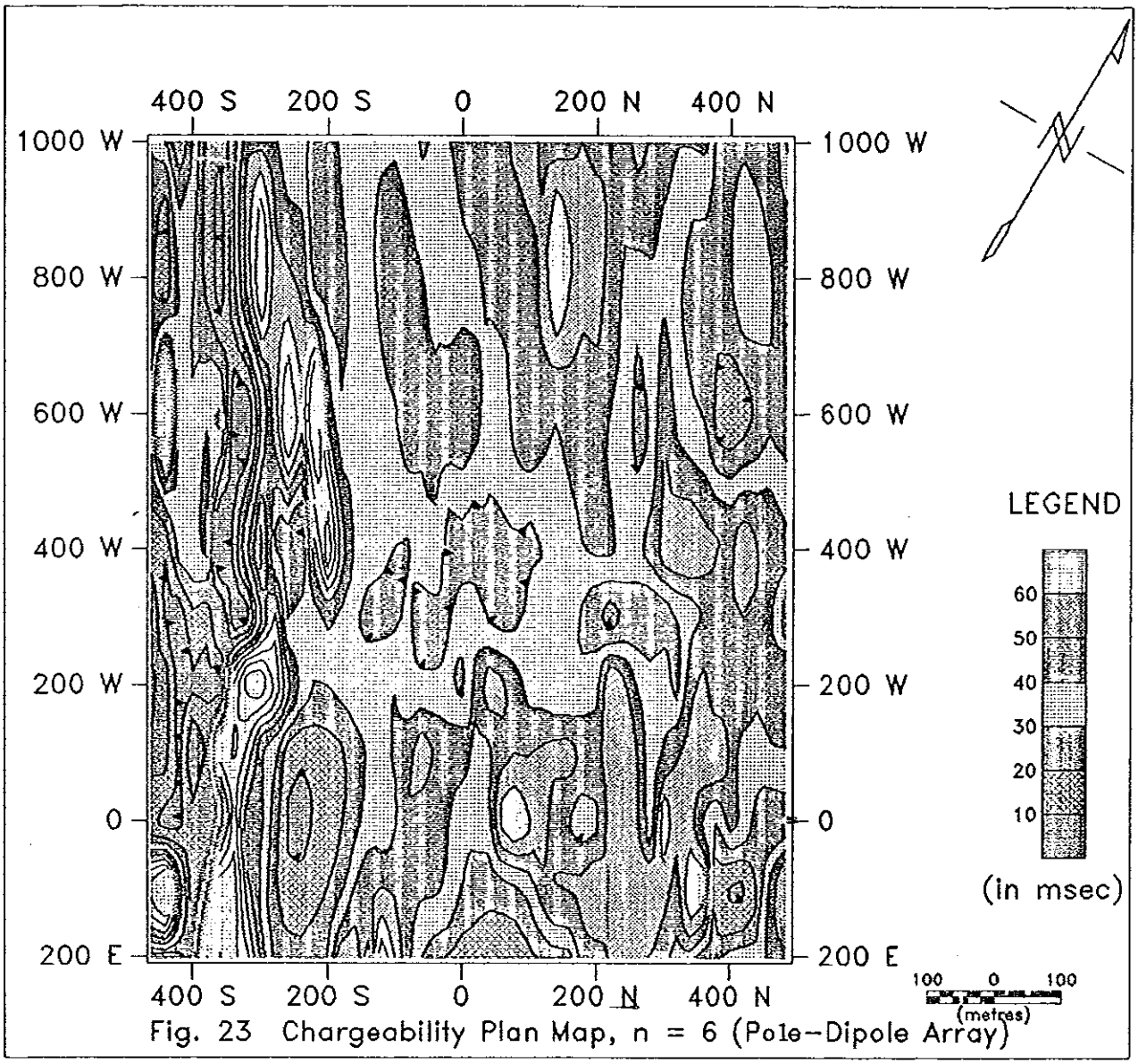

Fig. 23 Chargeability Plan Map, n = 6 (Pole–Dipole Array)

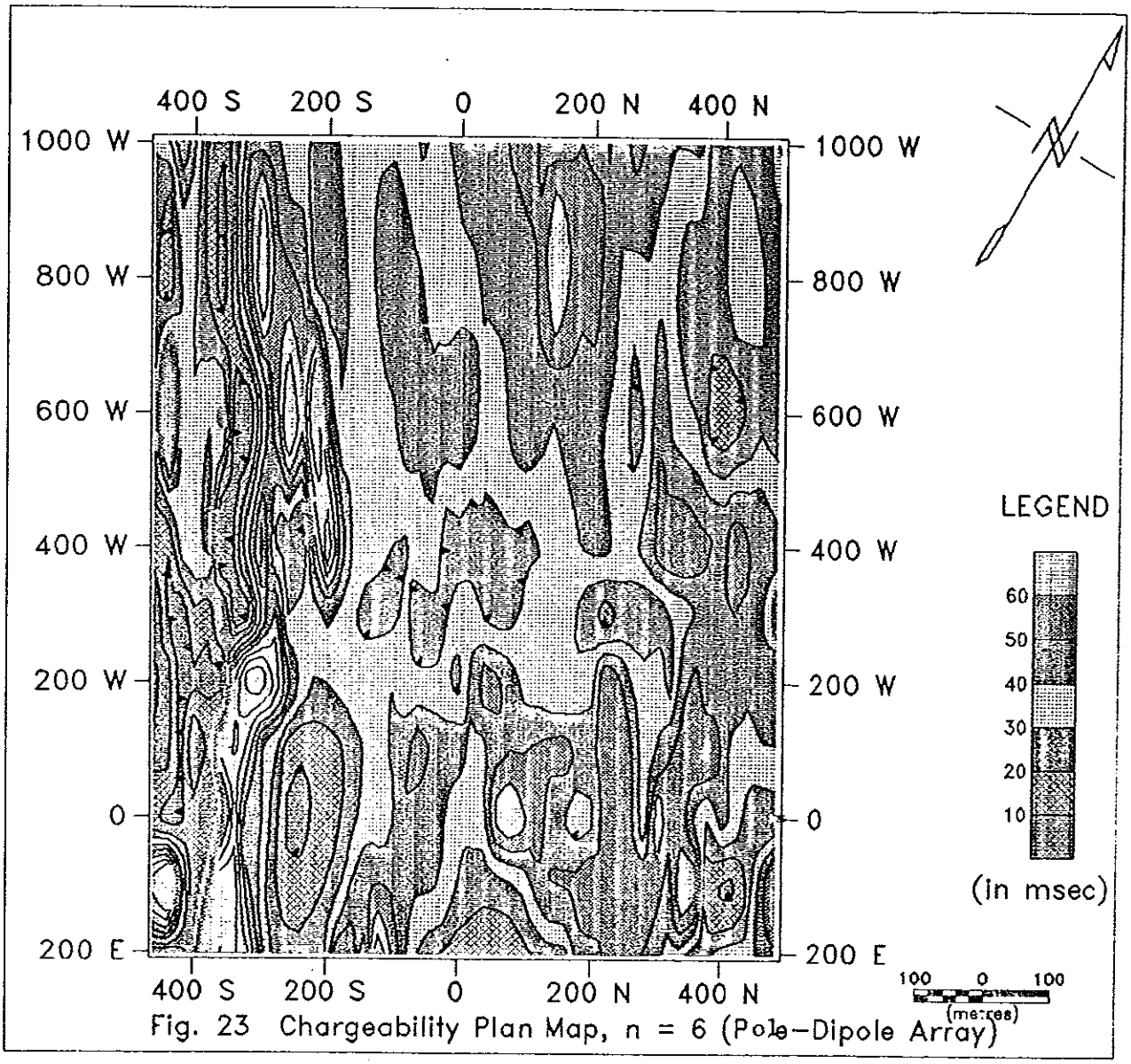

Fig. 23 Chargeability Plan Map, n = 6 (Pole–Dipole Array)

6. INTEGRATED ANALYSIS OF THE GEOPHYSICAL SURVEY DATA

The results of the individual geophysical surveys (radiometric, magnetic, electromagnetic, electrical resistivity and Induced Polarization) were presented in the preceding chapters on which basis the independent interpretations were made to account for the anomalies observed in each case.

In this concluding chapter, an integrated interpretation of the results of all the geophysical methods employed over the survey area is made.

6.1 Physico-geological Model

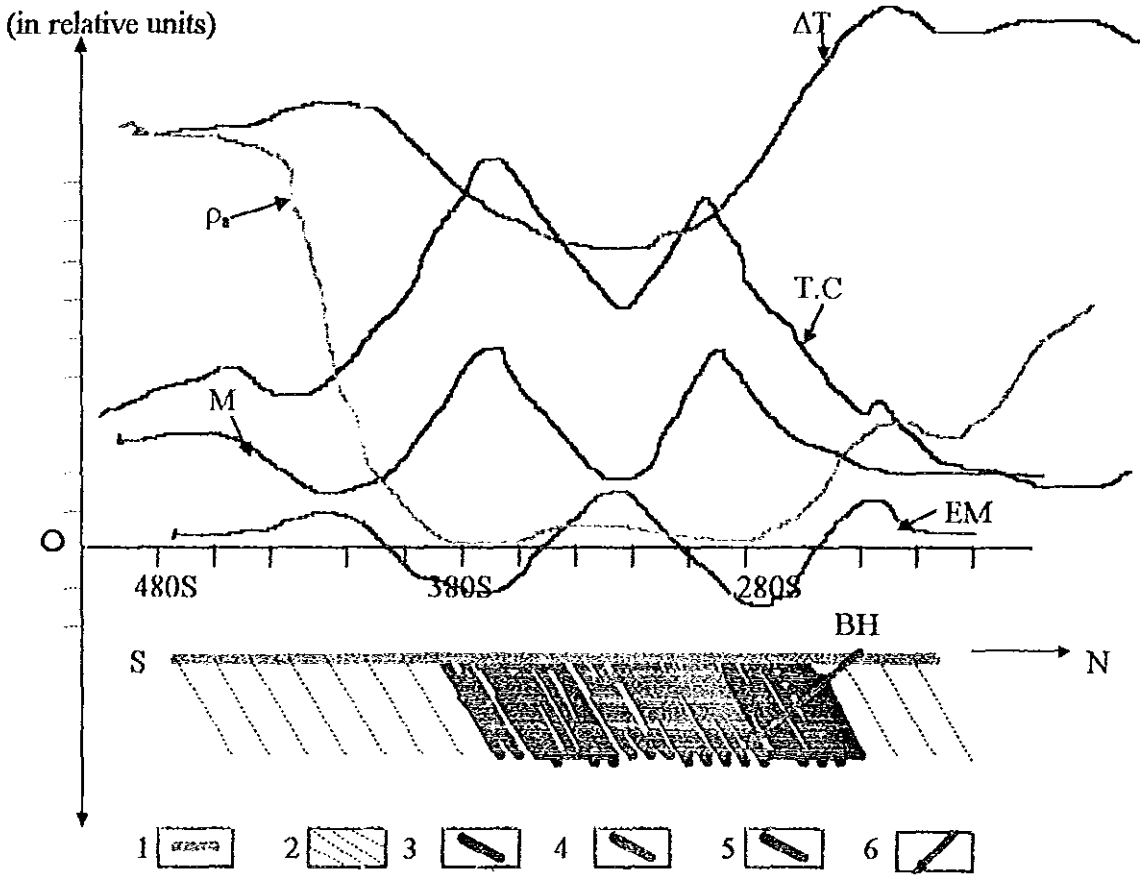

1 - overburden ;2 - mafic-ultramafic; 3 - quartzite; 4 - quartz-mica schist; 5 -graphitic schist; 6 - recommended bore hole location.

Fig. 24. Generalized Physico-Geological Model of the Gara-Gedemsa graphite occurrence.

6. INTEGRATED ANALYSIS OF THE GEOPHYSICAL SURVEY DATA

The results of the individual geophysical surveys (radiometric, magnetic, electromagnetic, electrical resistivity and Induced Polarization) were presented in the preceding chapters on which basis the independent interpretations were made to account for the anomalies observed in each case.

In this concluding chapter, an integrated interpretation of the results of all the geophysical methods employed over the survey area is made.

6.1 Physico-geological Model

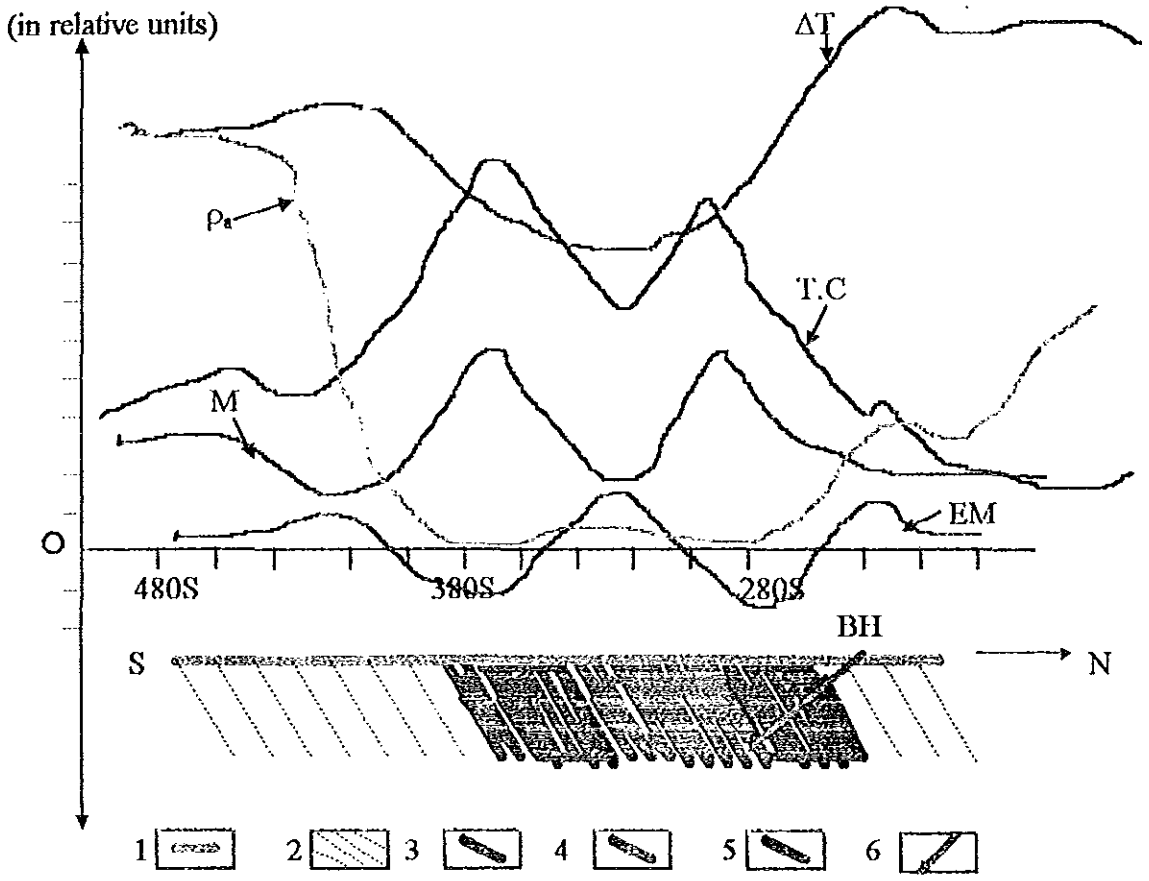

1 - overburden ;2 - mafic-ultramafic; 3 - quartzite; 4 - quartz-mica schist; 5 -graphitic schist; 6 - recommended bore hole location.

Fig. 24. Generalized Physico-Geological Model of the Gara-Gedemsa graphite occurrence.

6. INTEGRATED ANALYSIS OF THE GEOPHYSICAL SURVEY DATA

The results of the individual geophysical surveys (radiometric, magnetic, electromagnetic, electrical resistivity and induced polarization) were presented in the preceding chapters on which basis the independent interpretations were made to account for the anomalies observed in each case.

In this last and concluding chapter, an integrated interpretation of the results of all the geophysical methods employed over the survey area is made.

6.1 Physico-geological Model

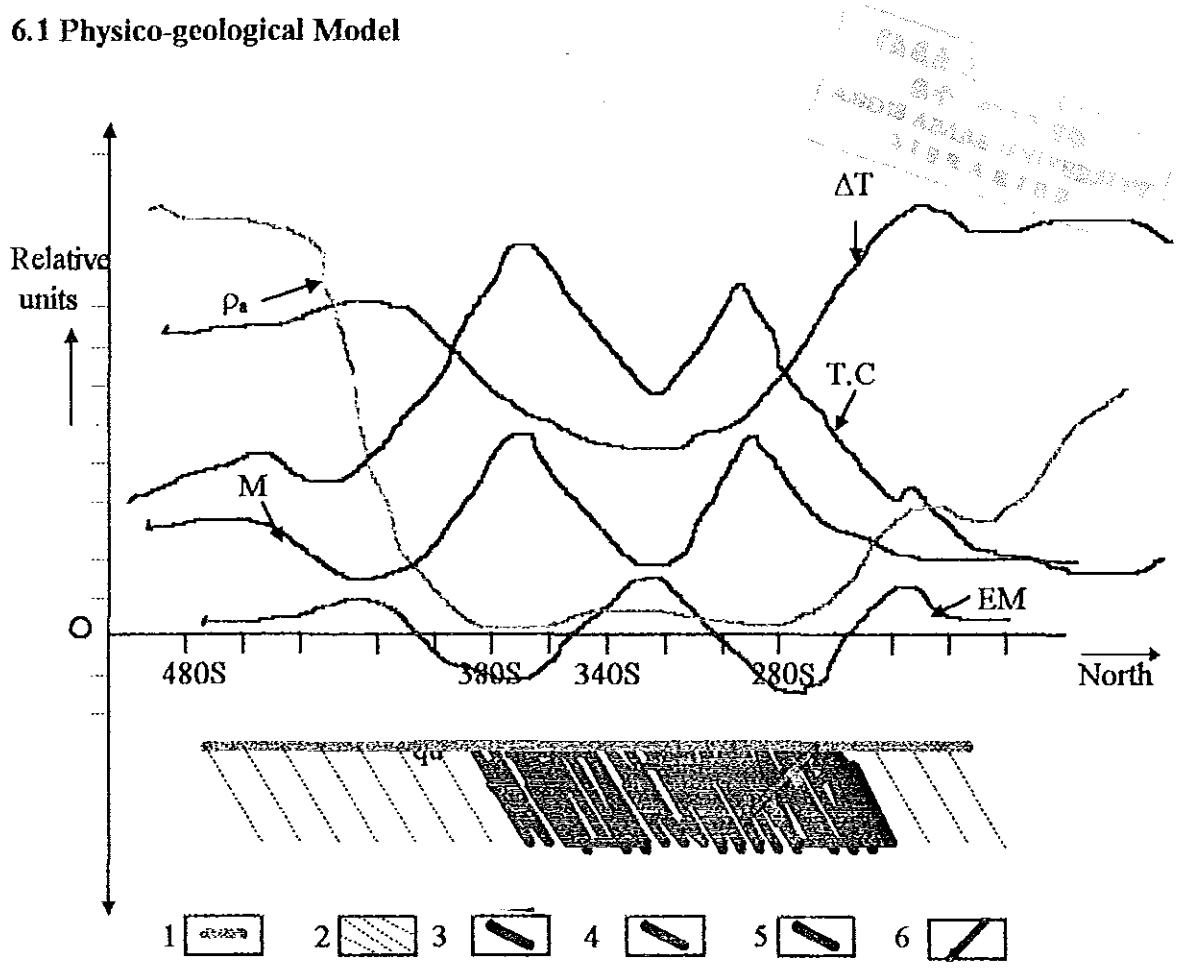

1 - overburden ;2 - mafic-ultramafic; 3 - quartzite; 4 - quartz-mica schist; 5 -graphitic schist; 6 - recommended bore hole location.

Fig. 24. Generalized Physico-Geological Model of the Gara-Gedemsa graphite occurrence.

Fig. 24 shows the generalized model of the Gara Gedemsa graphite occurrence and the features of the geophysical responses over the graphitic zone. As shown on the model, the mineralization zone is characterized by high radiometry, high IP and high EM anomalies, as well as low apparent resistivities and weak magnetic field intensities. According to the model, the source of the geophysical anomalies are parallelly dipping graphitic bodies which occur sandwiched in the host rocks.

Rough petrophysical analysis conducted using rock samples from the study area has revealed that both the graphitic schist and the host rocks display low magnetic susceptibilities. However, as compared to the host rocks represented by quartzite, pegmatite, and mafic-ultramafic units (talc-tremolite, talc-tremolite-actinolite and amphibole schists), over the graphitic mineralized zones the measured fields are found to show lower magnetic intensities and apparent resistivity and stronger chargeability. This fact is more or less shown on the physico-geological model (Fig. 24).

6.2 Discussion

The low magnetic field intensity, the high conductivity and high chargeability of the graphitic zones as compared to that of the host rocks are markedly reflected on the geophysical survey results. The pegmatite veins which are known to have space relationship with graphite mineralization also made possible the application of the radiometric method to indirectly delineate the graphitic mineralized zones. This is clearly observed on the total count and potassium contour maps, Figs. 3 and 4, where the mineralized zones are identified with their strong radioactive responses. Moreover, owing to the difference in the content of radioactive elements in rocks, the method has outlined the boundaries of the lithologic units distributed within the area of survey.

The geophysical results have mapped two prominent anomalous zones, among which the major one is outlined at the extreme southern part of the grid, whereas the second one mapped at

depth which may indicate more concentration of the causative body at depth. Therefore, this could be considered as a minor source of graphite mineralization from exploration point of view.

In addition to the two anomalous zones, the geophysical results have indicated so anomaly at the northwest of the grid which is characterized by high resistivity and moderate to h radiometry and chargeability responses. The IP and resistivity highs of this zone are also observ at depth with similar trend on the pole-dipole plan map for the maximum spacing (Figs. 19 a 23). The moderate to high radiometry and chargeability responses of this zone may indicate th presence of disseminated graphite mineralization along with the pegmatite veins. On the othe hand, the overlapping IP and resistivity highs may be good indicator for quartz-sulphide-gold typ of mineralization. This zone needs further geological follow up to confirm the geophysical survey results.

The asymmetry of the EM curves, i.e., the positive shoulders being greater at the hanging wall side (Figs. 13 and 14) and the trends of the pseudosection contour lines (Figs. 18 and 22), suggest that the anomalous body of the survey area uniformly dips at about 50^0-60^0 to the north. As seen on the pole-dipole plan map for the dipole spacing of n = 6 (Figs. 19 and 23), the anomaly detected at the southern margin is relatively displaced to the right which could be attributed to the dipping of the graphitic body as it is shown on the generalized physico-geological model in Fig. 24.

The anomaly interruption observed on the gradient chargeability contour map (Fig. 21) along the main anomalous zone could be explained interms of the potential distribution in or over the ground and the configuration of the method. The fixed spacings employed in the configuration for the current and potential electrodes have limited the resolution of the method over the graphitic body. From eqn. 34, i.e., $V = I\rho/2\pi r$, for constant current I, as the resistivity ρ diminishes the potential V could be very small to be detected. Accordingly, the very low resistivity of graphite could make difficult the detection of the potential distribution over the graphitic body with the fixed

6.4 Recommendations

Based on the above conclusions, the following recommendations are forwarded:

1. The electromagnetic method is recommended to be preferably applied in other areas with similar physico-geological environment. The IP/Resistivity methods should be applied over the EM anomalies for better information on the lateral and vertical distribution of the anomalous body.
2. The radiometry method was found to be suitable for geological mapping, and could preferably be applied for similar purpose in other areas with similar geological settings.
3. From exploration point of view, the anomalous body delineated at the southern margin of the grid is recommended to be followed up as a main source of graphite.
4. Accordingly, to confirm the results of the geophysical surveys and to further evaluate the economic significance of the inferred graphite mineralization, two bore holes are recommended over the main anomalous zone mapped at the southern margin of the survey grid. The bore holes are recommended to be drilled at 600W/250S and 600E/440S. Provided that the outcomes of the first drillings are promising, another bore hole is recommended to be drilled over the central anomalous zone at 0/100N. All bore holes are recommended to be sunk at 210^0 azimuth with 35^0 inclination as shown in Fig. 24.
5. Geological follow up is recommended at the northwest of the grid, where high IP and high resistivity anomalies are detected, because such anomalous zone may be a favorable site for quartz-sulphide-gold type of mineralization. In addition, the EM anomalies detected at the south beyond the current grid, parallel to the main anomalous zone, needs geological follow up and the application of other geophysical methods, like SP and IP/Resistivity, to confirm the result obtained with the EM survey.

LIST OF REFERENCES

[1] Brass, G., H. Flathe, and R. Scholz : Resistivity Profiling with different electrode arrays over a graphite deposit, *Geophysical Prospecting*, 29, 589-600, 1981.

[2] Breiner, s.: "Applications Manual for Portable Magnetometers." Geometrics, California, 1973

[3] Dobush, T.: The use of Integrated VLF/Magnetometer System in mineral exploration, *Technical Information*, Scintrex, California

[4] Dorbin, M.B.: "Introduction to Geophysical Prospecting," McGraw-Hill Company, USA, 1976.

[5] Dorbin, M.B., and C.H. Savit: "Introduction to Geophysical Prospecting," McGraw-Hill Company, New York, 1988.

[6] Gautneb, H.: A Brief Petrographic Study of Graphite Ore from the Moyale Area, Southern Ethiopia, *Geological Survey of Norway (NGU)*, Report 97 - 005, 1977.

[7] Gerkens, T.C.: "Foundation of Exploration Geophysics." Elsevier Scientific Publishing Company, Amsterdam, 1989.

[8] Goodwin, W.L.: "A handbook of prospecting," Industrial and Educational publishing co., Ontario, 1923.

[9] Gurevich, A.: "Prospecting for minerals," Translated from Russian, Foreign Languages Publishing House, Moscow, 1964.

[10] Heiland, C.A.: "Geophysical Exploration," Prentice-Hall, Inc., New York, 1946.

[11] Interpretational manual: IGS-2/EM-4 and SE-88 Moving Source GENIE, geophysical and geochemical instrumentation and services, Ontario, 1986.

[12] Keller, G.V., and F.C. Frischknecht: "Electrical methods in Geophysical Prospecting," Pergamon press, Oxford, 1966.

[13] Kuzvart, M., and M. Bohmer: "Prospecting and Exploration of Mineral Deposits," Elsevier Scientific Publishing Company, Amsterdam, 1978.

[14] Nettleton, L.L.: "Gravity and Magnetics in Oil Prospecting," McGraw-Hill Book Company, New York, 1976.

[15] Operation Manual: Mp-3/4 Proton magnetometer systems, geophysical and geochemical instrumentation and services (Scintrex), 1988.

Appendix B

Assume a point electrode delivering I amperes located at the surface of a semi-infinite homogeneous isotropic medium and the air above it has zero conductivity. The current circuit is completed through another electrode, usually at surface, placed far enough away that its influence is negligible.

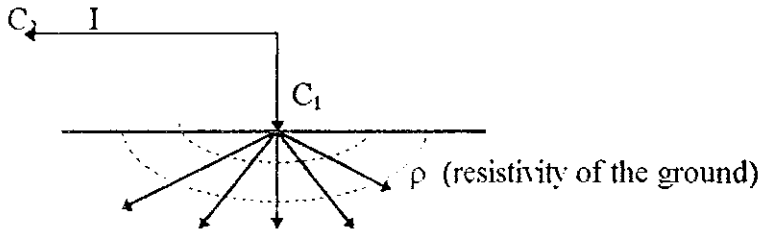

Fig. 26 Point source of current at the surface of a homogeneous medium

From the symmetry of the system, the potential will be a function of r only, where r is a distance from the point electrode c_1. Thus Laplace's equation in spherical coordinate becomes

$$\nabla^2 V = \frac{d^2V}{dr^2} + \frac{2}{r}\frac{dV}{dr} = 0$$

Multiplying both side by r^2 and integrating, we obtain

$\frac{dV}{dr} = \frac{A}{r^2}$, where A is integration constant

Integrating again, we get

$V = -\frac{A}{r} + B$, where B the second integration constant

Applying boundary conditions:

i) V vanishes as r increases to infinite. i.e., B = 0

ii) $\frac{dV}{dr} = 0$ at z = 0 because $\sigma_{air} = 0$

and defining $I = 2\pi r^2 J$, where $J = -\sigma\, dV/dr$ from eqns. (32) and (33), is current density, the integration constant A is evaluated by

$$A = -\frac{I\rho}{2\pi}$$

Substituting for A in equation for V above, a potential due to a single current electrode a distance r from it is obtained as

$$V = \frac{I\rho}{2\pi r}$$

DECLARATION

I, the undersigned, declare that my thesis being entitled is my original work and has not presented for a degree in any other University. Sources of relevant materials taken from books and articles have been duly acknowledged.

Name: Alemna Jaleta

Signature: Alemna J.

This thesis has been submitted for examination with my approval as University advisor.

Name: TIGISTU HAILE

Signature: Tigistu Haile

Date: 18 Dec 1997

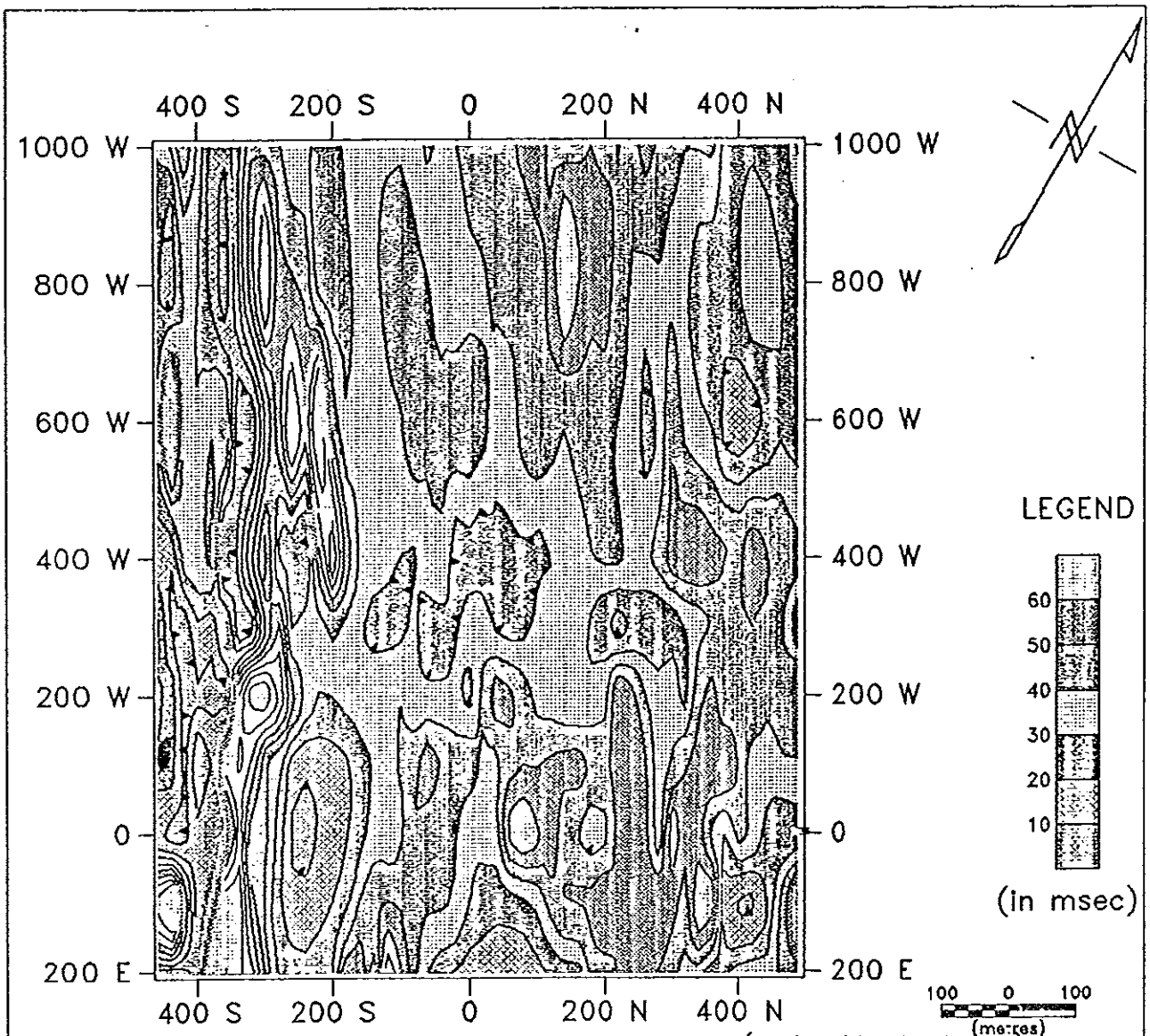

Fig. 23 Chargeability Plan Map, n = 6 (Pole–Dipole Array)

ADDIS ABABA UNIVERSITY

School of Graduate Studies

Application of Integrated Geophysical Methods for Graphite Exploration in Gara Gedemsa Area (Moyale, Southern Ethiopia)

by

Alemna Jaleta

Faculty of Science

Approved by: Board of Examiners

Dr. Tigistu Haile	
Advisor	
Dr. Getnet Mewa	
Co-advisor	
Ato Girma W/Tinsae	
External Examiner	
Dr. Fekadu Kebede	
Internal Examiner	
Dr. Solomon Tadesse	
Chairman	